JPET Fast Forward. Published on April 20, 2010 as DOI: 10.1124/jpet.110.168526

JPET 168526

Title Page

Tracing Multiscale Mechanisms of Drug Disposition in Normal and Diseased Livers

Sunwoo Park, Sean H.J. Kim, Glen E.P. Ropella, Michael S. Roberts,

and C. Anthony Hunt

The Department of Bioengineering and Therapeutic Sciences, Biosystems Group, University of California,

San Francisco, CA, USA 94143: SP, GEPR, CAH

The UCSF/UCB Joint Graduate Group in Bioengineering, University of California,

San Francisco, CA, USA 94143: SHJK, CAH

Tempus Dictum, 3315 SE 19th Ave., Suite F, Portland, OR, USA 97202: GEPR

School of Medicine, Princess Alexandra Hospital, University of Queensland, Woolloongabba, Queensland,

4102, Australia: MSR

JPET Fast Forward. Published on April 20, 2010 as DOI: 10.1124/jpet.110.168526
This article has not been copyedited and formatted. The final version may differ from this version.

Running Title Page

Running title: Micromechanisms of Drug Disposition in Health and Disease

Corresponding author:

C. Anthony Hunt

Department of Bioengineering and Therapeutic Sciences

University of California, 513 Parnassus Ave., S-926

San Francisco, CA 94143-0446

P: 415-476-2455; F: 415-514-2008

<a.hunt@ucsf.edu>

Number of text pages: 21

Number of figures: 8

Number of tables: 1

Number of references: 26

Words in Abstract: 221

Words in Introduction: 678

Words in Discussion: 1,394

Abbreviations:

ALC: alcohol; CCl_4: carbontetrachloride; CV: central hepatic vein; ISL: In Silico Liver; PK: pharmacokinetic; PV: terminal portal vein tracts; SM: Similarity Measure; SS: Sinusoidal Segment

JPET Fast Forward. Published on April 20, 2010 as DOI: 10.1124/jpet.110.168526
This article has not been copyedited and formatted. The final version may differ from this version.

Abstract

Hepatic drug disposition is different in normal and diseased livers. Different disease types alter disposition differently. What are the responsible micromechanistic changes and how do they influence drug movement within the liver? We provide plausible, concrete answers for two compounds, diltiazem and sucrose, in normal and two different types of cirrhotic rat livers: chronic pretreatment of rats with CCl_4 and alcohol caused different types of cirrhosis. We started with simulated disposition data from normal, multilevel, physiologically based, object-oriented, discrete event In Silico Livers (normal ISLs) that validated against diltiazem and sucrose disposition data from normal livers. We searched the mechanism's parameter space and found three parameter vectors that enabled matching the three wet-lab data sets. They specified micromechanistic transformations that enabled converting the normal ISL into two different types of diseased ISLs. Disease caused lobular changes at three of six levels. The latter provided in silico disposition data that achieved a prespecified degree of validation against wet-lab data. The in silico transformations from normal to diseased ISLs stand as concrete theories for disease progression from the disposition perspective. We also developed and implemented methods to trace objects representing diltiazem and sucrose during disposition experiments. So doing enabled providing heretofore-unavailable insight into plausible disposition details in normal and diseased livers. We posit that changes in ISL micromechanistic details may have disease-caused counterparts.

JPET Fast Forward. Published on April 20, 2010 as DOI: 10.1124/jpet.110.168526
This article has not been copyedited and formatted. The final version may differ from this version.

Introduction

Liver cirrhosis alters hepatic drug disposition complicating drug therapy management (Dourakis, 2008; LaCouteur et al., 2005). The nature of alterations is dependent on both the cause and the extent of disease. Improved mechanistic insight is needed on two fronts. We need supported, concrete theories for 1) how a drug's interaction with the hepatic micro-architecture contributes to overall measures of disposition and 2) how disease progressively alters those micro-architectural features. Achieving both is complicated by the heterogeneity of hepatic micro-architectural features (for examples and a discussion, see (Liu et al., 2007)), and differences in cirrhosis. We focus on two standard rat models of cirrhosis: chronic treatment with 1) carbon tetrachloride (CCl_4) and 2) ethanol (Hung et al. 2002a,b). In advanced stages, CCl_4 treatment produces acute hepatocellular injury with centrilobular necrosis and stenosis. In contrast, chronic alcohol treatment produces hepatocellular injury with inflammation and perivenular macrovesicular steatosis (fatty degeneration). Both treatments cause fibrosis.

We report significant progress in achieving both objectives by developing, refining, validating, and experimenting on discrete, object and agent-based In Silico Livers (ISLs). ISLs are works in progress. Observable micromechanisms in ISLs map directly to wet-lab counterparts, which facilitates the falsification of hypotheses about those mechanisms. See Hunt et al. (2009) for complete descriptions of the modeling method. We matched disposition profiles from ISLs and from in situ perfusion experiments in normal rat livers for diltiazem and sucrose. Matches were achieved through cycles of iterative ISL refinement that narrowed the space of plausible, spatially distributed, micromechanisms. Many future ISL iterations are likely. Nevertheless, we discovered a limited set of ISL changes that produced profiles that acceptably matched in situ experiments on the two types of diseased livers (Hung et al., 2002a,b). Diseased ISLs were created independently.

Parameterizing detailed multi-zone versions of familiar physiologically based pharmacokinetic models has proven challenging because of hepatic heterogeneity coupled with interindividual variability (Liu et al., 2007). We pursued a fundamentally different approach. A dictum of the physicist Richard Feynman was "what I cannot create, I do not understand." Uncertainty is large and detailed data are limited for micromechanisms that are responsible for differences in hepatic disposition profiles. Hence, it follows that to gain insight, we need to build extant (actually existing, observable), working mechanisms that exhibit

some of those same phenomena. We must construct, validate, and explore analogue mechanisms and tissues in order to better understand the biological counterparts. We built extant biomimetic mechanisms and tissues using object-oriented software tools. In doing so, we were not building a model using published biological facts, ideas, and assumptions. Rather, we constructed reasonably realistic, biomimetic mechanistic hypotheses. We then explored and shrank the space of the resulting disposition profiles to achieve a prespecified similarity to wet-lab profiles.

Our focus was on constructing and falsifying plausible biomimetic mechanisms at multiple levels. We argue that the causative, mechanistic details executed in ISLs may have wet-lab hepatic counterparts during diltiazem disposition, as diagrammed in pair A of Fig. 1. Differences in mechanistic details between normal and the two "diseased" ISLs (pair B in Fig. 1) are hypotheses about corresponding differences between the normal and diseased livers. Simulation enables testing those hypotheses. Achieving a degree of profile matching is evidence supporting those hypotheses. The differences in dynamic, multilevel details during execution provide plausible explanations of differences between the two disease models. Simulations of transformations of normal into diseased ISLs stand as abstract theories for disease progression: similar transformations may have occurred in rats during disease progression.

An important advantage of this class of models is that micromechanistic details are observable, unlike real livers. Methods were implemented to trace, measure, and record changes in dynamic spatiotemporal details. So doing provided a heretofore-unavailable view of how and where micromechanistic events combine to influence disposition within ISLs. We posit that changes in micromechanistic details from normal to diseased ISLs may have disease-caused hepatic counterparts. These methods are extensible to whole organisms and, eventually, patients. Hence, they open a door to new experimental means of testing the plausibility of mechanistic explanations. That is expected to facilitate translation of research results to benefit patients.

Methods

Rationale for modeling and simulation approach. Classical physiologically based PK modeling (Hung et al., 2001, 2002a,b) provide examples and the approach used herein, although fundamentally different, are complementary approaches to gaining insight into plausible mechanisms responsible for PK data. The former provides a conceptual generalization, a global description of flow, influx, efflux, binding,

JPET Fast Forward. Published on April 20, 2010 as DOI: 10.1124/jpet.110.168526
This article has not been copyedited and formatted. The final version may differ from this version.

sequestration, and metabolism, and relates the resulting parameter values conceptually to observed changes in liver pathophysiology and biochemistry. Neither the model nor its parameters can be made realistic and similar to hepatic features (Rescigno, 2001). The synthetic method of modeling and simulation is fundamentally different (Hunt et al., 2009). The method enables ISLs to use actual mechanisms—events occurring within specified spaces—in a manner that is more consistent with the actual intralobular arrangements, normal and pathological, than is possible using traditional mathematical models. An ISL instantiates a hypothesis (Fisher and Henzinger, 2007; Hunt et al., 2008). Execution and comparison of results to referent counterparts tests the hypothesis. The relationship between ISL spaces, components, mechanisms, and phenomena—mappings 1–3 in pair A of Fig. 1—can be made increasingly realistic and similar to hepatic counterparts. Doing so is facilitated by grounding the internals of the ISL relative to each other rather than to absolute metric units like seconds or meters. Relative grounding makes the causal effects of changes to any one component evident as they ripple through the entire model and are measured by an observer. This capability dramatically increases the extent to which a model can be refined and translated to other contexts. For a discussion of Grounding, see (Hunt et al., 2009). For convenience a brief discussion of how grounding influences differences between differences between traditional, inductive, equation based PK models (left side of Fig. 1) and synthetic, internally grounded analogues like ISLs In provided in Supplementary Discussion in Supplementary Material.

Most ISL form and function details used herein are the same as used earlier (Park et al., 2009). A dense, abridged description follows. Some of the tracing features, detailed in Supplementary Material, are new. Included is a discussion and example of technical issues related to the granularity of the tracing and the granularity of the computation. For convenience, parameter descriptions are also provided in the Appendix. Detailed descriptions of ISL design considerations, including ISL-to-liver mappings are available (Hunt et al., 2006; Yan et al., 2008a,b; Park et al, 2009). ISL mechanistic details are presented as plausible approximations of what actually occurred. To avoid conflating ISL details with the biology, and to clearly distinguish in silico components and processes from hepatic counterparts, hereafter we use SMALL CAPS when referring to the ISL counterparts.

In Situ Liver perfusion studies. Full details of the original single-pass, liver perfusion experiments along with an explanation for the choice of compounds studied are provided by Hung et al (2001, 2002a,b). Included are descriptions of two established methods to induce fibrotic, hepatic cirrhosis in rats (150g male

JPET Fast Forward. Published on April 20, 2010 as DOI: 10.1124/jpet.110.168526
This article has not been copyedited and formatted. The final version may differ from this version.

Wistar). Normal and two types of diseased livers were studied. Similar pretreatment protocols were used to create the eight diseased livers for each group: one group was produced by chronic CCl_4 treatment; the other by chronic alcohol (ethanol) treatment. Both protocols induced acute hepatocellular injury, but their histologies were different. Each model type reflects different aspects of human disease. Control, normal pharmacokinetic (PK) profiles were obtained using livers from matched rats treated identically, absent either CCl_4 or alcohol treatment. Several histopathology measures characterized the nature and extent of disease. Nine outflow profiles of coadministered diltiazem and sucrose were analyzed individually using established PK methods. The referent data are presented in Fig. 1 of Hung et al. (2002b)

An ISL is a simulation framework: an in silico counterpart to an entire wet-lab experimental system (analytical instrumentation and all). It comprises an experiment agent, a data management module, a statistical observer module (used to analyze data), a parameter manager, plus data from the perfusion experiments (and interpolations, when needed), *RefModel*, and LOBULE. *RefModel* is the parameterized, classical PK model, which was fit by Hung et al. (2002a) to the wet-lab data. Concurrent execution of it and an ISL enabled judging similarities or lack thereof during iterative ISL refinement (discussed below). *RefModel* is a two-phase stochastic liver model (stochastic PK model hereafter): it predicts the time course of diltiazem in liver effluent during a perfusion experiment that follows a standardized dosing protocol. Its implementation is provided in Supplementary Material.

A LOBULE is one Monte Carlo variant of the complete system illustrated in Fig. 2. Three LOBULE variants (NORMAL and two DISEASED) were developed in parallel. For simplicity, we began by assuming that anatomical, physiological, and PK characteristics of all hepatic lobules within a specific liver, normal and diseased, are somewhat similar (Hunt et al, 2006; Yan et al., 2008a). Pooled and averaged results from ISL executions of 48 Monte Carlo variants of a single, parameterized LOBULE represents a single wet-lab outflow profile; those results comprise one ISL experiment.

Figure 2 shows that LOBULES are abstractions: they are not intended to be accurate, precise descriptions of hepatic physiology. ISL components can be modified and plugged together in different ways as needed to represent different lobular properties or the consequences of disease. ISL experiments help reduce uncertainties about hepatic mechanisms by enabling the formulation and testing of fine-grained mechanistic hypotheses about plausible, fine-grained mechanistic details that may be occurring during drug disposition (Hunt et al, 2009). Software objects represent spatiotemporal aspects of hepatic organization and function.

JPET Fast Forward. Published on April 20, 2010 as DOI: 10.1124/jpet.110.168526
This article has not been copyedited and formatted. The final version may differ from this version.

The consequences following execution are measured and studied simultaneously, analogous to how wet-lab experiments are conducted. An ISL—NORMAL or DISEASED—achieves a degree of validation when the similarity between its outflow profile and a referent perfusion profile is judged adequate based on some quantitative comparison. Once that has been achieved, we state that the mappings marked 2 in pair A of Fig. 1 are plausible. As recently discussed (Hunt et al, 2009), a LOBULE should be no more complicated than is needed to achieve the stated objective. For this study, the objective has been to discover a minimal set of NORMAL ISL parameter changes that will lead to DISEASED ISLs that achieve a degree of validation against referent outflow profiles.

When ISL components and their arrangement are judged acceptable, the detailed micromechanisms causing traceable events may correspond to the hepatic micromechanisms; i.e., mappings 1 in Pair A of Fig. 1 are plausible. At that stage, the traced DILTIAZEM and SUCROSE dynamics within and between an ISL's six levels provide heretofore-unavailable insight into plausible drug disposition details.

A LOBULE is a network of sinusoidal segments. The relative arrangement of hepatic function and blood flow is represented at the LOBULE level using a directed graph called a SINUSOID network. Each Monte Carlo variant maps to a distinct arrangement of flow paths from portal vein tracts (PV) to the central vein (CV) within a portion of an acinus. A SINUSOID network is subdivided into three zones. Zonation enables mimicking quantitative and functional differences between periportal and perivenous lobular regions (Miller et al., 1979; Gumucio and Miller, 1982; Gaudio, 1992). It is a means of achieving an adequate variety of PV-to-CV flow paths. SINUSOID network structure properties are specified as a topology of nodes and edges. The number of nodes per Zone is always Zone 1 > Zone 2 > Zone 3. A graph edge specifies a flow connection from a Sinusoidal Segment (SS) exit to a downstream SS entrance. Having edges assigned pseudo-randomly at the start of each ISL experiment simulates lobular variability within and between livers.

A SS is a software agent (an autonomous object that schedules its own events and interacts with other agents and objects in its environment) that represents all aspects of sinusoid function that can influence drug disposition. One SS is assigned to each graph node. Each is somewhat different and the stochastic differences are parameter controlled. SSs per zone were Zone 1 = 45, Zone 2 = 20, and Zone 3 = 5. As previously explained (Yan et al. 2008a), those numbers were needed to have sufficient PV-to-CV path variety to reduce fluctuations within outflow profiles. They were connected using a minimum of 109 edges: 39 intra-Zone 1 edges, 8 intra-Zone 2 connections (but no intra- Zone 3 connections), 37 Zone 1-to-Zone 2,

JPET Fast Forward. Published on April 20, 2010 as DOI: 10.1124/jpet.110.168526
This article has not been copyedited and formatted. The final version may differ from this version.

and 25 Zone 2-to-Zone 3 connections. All Zone 3 nodes were connected to CV. There were two constraints: no self-self edges and no two-node cycles (a restriction that was not imposed earlier (Hunt et al., 2006;Yan et al., 2008a,b)), and if any node was, by chance, not assigned an outgoing edge, it was connected directly to CV. Two SS types were used: direct (larger, shorter; controlled by the *DirSin* parameters in Table 1) and tortuous (thinner, longer; controlled by the *TortSin* parameters in Table 1).

A SS consists of a Core and three identically sized layered toroidal spaces as illustrated in Fig. 2. Spaces A–C within a SS are identical, but SS sizes (Table 1) are Monte Carlo specified. The spaces are subdivided into a parameter specified number of square grid spaces. The Core maps to blood flow. It provides a direct PV-to-CV path through which COMPOUNDS (mobile objects) can traverse. Space A maps to the interface between vascular flow and the endothelial layer. Space B is called the ENDOTHELIAL layer. It maps to easily accessible spaces and cells presumed to be primarily endothelial cells and fenestrae. Space C is called the HEPATOCYTE layer. It maps to less accessible spaces and cells, primarily the space of Disse, hepatocytes, and bile canaliculi. CELLS in Space B are called ENDOTHELIAL CELLS; those in Space C are called HEPATOCYTES. Parameters allow the resolution of the spaces to be changed as needed. A Bile Space, not illustrated in Fig. 2, can be added when needed.

CELLS contain whatever objects are needed to represent *required* intracellular processes, such as drug binding, metabolism, transport, and sequestration. Because the in situ perfusions had short durations (less than one hour), we assume that cell biology and biochemistry were relatively constant. Consequently, details not needed are abstracted away, but can be added easily when needed (Hunt et al., 2006; Yan et al., 2008a; Park et al., 2009). It is known that basic compounds such as diltiazem are sequestered in organelles such as lysosomes and mitochondria, as well as being bound to intracellular material (Hung et al., 2002a; Siebert et al., 2004). However, motivated by parsimony, sequestration and binding are not resolved: everything within a cell that can bind or sequester diltiazem is conflated and represented by some number of identical binding objects (hereafter, simply BINDERS). Within hepatocytes, we do not resolve binding to metabolic enzymes, such as the CYP450 isozymes, and binding to or sequestration by other cell components. BINDERS called ENZYMES handled BINDING inside HEPATOCYTES. They use a parameter (*metabolizeProb*) to determine which of their BINDING events ends with release of METABOLITE. When needed, several different objects that produce the same net event sequence can replace a BINDER ENZYME.

ISL parameters. As in Park et al. (2009), ISLs were iteratively refined (Hunt et al., 2009) to achieve a

JPET Fast Forward. Published on April 20, 2010 as DOI: 10.1124/jpet.110.168526
This article has not been copyedited and formatted. The final version may differ from this version.

set of targeted attributes along with a rigorous degree of prespecified similarity with referent outflow profiles. An illustration of iterative parameter adjustment is provided in Supplementary Material. No new attributes, other than the additional disease-altered outflow profiles were added. ISL parameters specify structural and functional properties, experiment configuration, and DOSE. The ISL and its components from earlier work were re-used (Yan et al., 2008a; Park et al., 2009).

MonteCarloRuns: An ISL experiment averages 48 Monte Carlo trials (LOBULE). Execution duration in simulation cycles is specified by *cycleLimit*. The number of steps executed each cycle is *stepsPerCycle*. DRUG disposition is observed at cycle resolution; spatiotemporal activities are traced at step resolution. One simulation cycle maps to 0.5 seconds and a step maps loosely to 0.25 seconds. *CycleLimit* and *stepsPerCycle* were set to 200 and 2, respectively. *ExperAgent* is absolutely grounded, whereas LOBULES are not. A technical issue dealing with how time is discretized at the simulation cycle and step levels in discussed in Supplementary Material.

Parameters named in this paragraph govern structural and spatiotemporal properties. *GraphSpecFile* is used to create a LOBULE'S sinusoidal network at the start of each simulation. *DirSinRatio* and *TortSinRatio* specify the ratio of the two SS types. SS circumference and length are generated using the values of *DirSinCircMin/Max*, *TortSinCircMin*/*Max*, *DirSinLenAlpha/Beta*/*Shift*, and *TortSinLenAlpha*/*Beta/Shift* (Hunt et al., 2006; Yan et al., 2008a,b). A2B/B2A/B2C/C2BJumpProb governs probabilistic COMPOUND movement. Simulated blood flow (in the Core) and local, biased random walk (Spaces A-C) are controlled by *CoreFlowRate* and *SinusoidTurbo*; their values can depend on the COMPOUND'S physicochemical properties. *ECDensity* and *HepDensity* specify the fractions of Spaces B and C occupied by ENDOTHELIAL CELLS and HEPATOCYTES, respectively. The numbers of BINDERS and ENZYMES within each CELL is Monte Carlo drawn within the range specified by *BindersPerCellMin/Max*. *SoluteBindingProb* designates the probability that a DRUG will be bound. Each binding event lasts *SoluteBindingCycle*s. The latter two parameters also depend on the COMPOUND'S physicochemical properties (Hung et al., 2001; Mager and Jusko, 2006).

MetabolizeProb is the probability that a METABOLITE, rather than DILTIAZEM, will be released from an ENZYME-DILTIAZEM complex. *ISLWetLabScaling* is a scaling factor used to map COMPOUNDS exiting CV directly to drug concentration (in perfusate). *MembraneCrossing* (valued 0,1) specifies whether a particular COMPOUND is allowed to enter CELLS.

JPET Fast Forward. Published on April 20, 2010 as DOI: 10.1124/jpet.110.168526
This article has not been copyedited and formatted. The final version may differ from this version.

Differences between NORMAL and DISEASED ISLs. The histopathology data showed that within both CCl_4-treated and alcohol-treated livers, significant cirrhotic change occurred at cellular and subcellular levels (Hung et al., 2002a,b). Microscopy evidence showed that microvascular and microcirculation changes occurred (Gaudio and Onori, 1997). For simplicity, many of the details known about liver fibrosis, including the principal role played by hepatic stellate cells, for example, were not added to the list of targeted attributes. It is tempting to assume that those visible changes must have contributed in important ways to the observed alterations in outflow profiles. Yet, we do not know the dispositional significance of such changes for specific compounds. We elected to make no inferences but seek one of the simpler sets of changes that could provide a plausible explanation. It may be possible, for example, that two different SINUSOID networks, with all cellular and subcellular details being unchanged, can provide an explanation for the differences. However, Hung et al. showed significant correlations between measures of histopathology and changed PK parameter values (Hung et al., 2002a,b). We therefore elected to begin by re-using the validated NORMAL LOBULE network structure the DISEASED LOBULE network structure. We then looked for explanatory change at the SS level and below. Note that when required, a validated simpler micromechanism can be made more complicated.

Starting with the validated NORMAL ISL (Park et al., 2009), the protocol of each refinement cycle followed three steps. That ISL provided a Similarity Measure (SM) > 0.8, discussed below. 1) We identified a subset of parameters to be changed (everything except the zonation, primary flow paths and their arrangement), and then sought focused changes in SS component parameterizations that would alter the outflow profile in ways consistent with the diseased outflow profile. More detail is provided in the *ISL implementation and execution* subsection. 2) We tested the hypothesis that a new valuation of the subset, in combination with unchanged values of all other parameters, would yield a ISL that could achieve SM > 0.8. When falsified, we returned to step one. 3) We fine-tuned the DISEASED ISL parameter vectors with the objective of achieving SM > 0.9 (within a factor of 0.33 of the referent value, as discussed below). When that failed, we returned to step one or two.

ISL parameter influences are not independent (Hunt et al., 2006) More than one parameter vector can give essentially indistinguishable outflow profiles (Yan et al., 2008a) Although every effort was made to construct a minimal model, the requirement that LOBULAR structures be derived or inferred from published hepatic knowledge rather than induced from particular data sets provides some complexity and overlapping

JPET Fast Forward. Published on April 20, 2010 as DOI: 10.1124/jpet.110.168526
This article has not been copyedited and formatted. The final version may differ from this version.

phenomena.

Drug input, dosage time management, and Similarity Measure. ISL experiments followed the same dosing protocol used in situ (Yan et al., 2008a,b; Park et al., 2009). As illustrated in Fig. 2, a bolus dose of SCUROSE and/or DILTIAZEM was injected into a simulated catheter that feeds into PV. COMPOUNDS were collected as they entered CV, simulating collection by a fraction collector. Details of dosing within the ISLs are provided in (Park et al., 2009) and for convenience in Supplementary Material.

An ISL outflow profile was accepted as valid—as being indistinguishable experimentally from a profile obtained from a repeat wet-lab experiment—when SM > 0.8. Once that was achieved, it was increased to SM > 0.9. ISL outflow profiles were compared with referent profiles using the quantitative SM used previously (Hunt et al., 2006; Yan et al., 2008a,b; Park et al., 2009). For convenience, details are provided in Supplementary Material. An ISL profile was acceptable as being experimentally indistinguishable when the fraction specified by the SM was within the ± 33% band around the referent values (Fig. 3).

ISL implementation and execution. ISLs were implemented within the high performance, computing infrastructure diagrammed in Supplementary Fig. S1 online. Its methods were designed to provide improved lifecycle management, execution efficiency, tracing quality, and analysis of traced results (Ropella et al., 2003). Each parallel mode was associated with one of the six ISL levels illustrated in Fig. 2 or an experimental requirement. Heterogeneity in parallel execution helped achieve improved performance along with efficient resource management. ISL parallel mode (Fig. S1), was supported at group and experiment levels. Group Level Parallel mode enabled executing multiple experiments in parallel by segregating each and allowing each to run concurrently without interaction. Parallel batch processing and analysis of local execution results were performed using that mode. Experiment Level Parallel mode enabled executing single experiments in parallel as separate LOBULE Monte Carlo variants.

Parallel parameter sweeping (Supplementary Fig. S1 online) was used to construct and explore regions of ISL parameter space for vectors that enabled the ISL outflow profile to meet or exceed the specified SM. The location of such a region was deduced by coupling prior ISL parameterization experience with physiologically based heuristics. The latter helped identify regions that contain abiotic parameterizations: the resulting ISL cannot map to a liver. Occasionally, a region was selected randomly. A global search of the entire parameter space was impractical.

Within the experiment framework, a simulation coordinator managed the overall simulation life cycle by

JPET Fast Forward. Published on April 20, 2010 as DOI: 10.1124/jpet.110.168526
This article has not been copyedited and formatted. The final version may differ from this version.

controlling the top-level agent, *ExperAgent*. It also supervised system components including the parallel parameter sweeper, parallel batch processor, parallel model partitioner, and model deployer. Their integration provided a fully automated, high-performance simulation environment within which all experiments were conducted. We built the environment using the tools specified in Supplementary Material.

Multiscale event tracing within ISLs during simulations. Tracing disposition events within and between ISL levels was divided into two phases: generating tracing data and then evaluating the data using quantitative measures. First, all spatiotemporal events involving COMPOUNDS (of the same type) across all ISL levels were stored. Tracing measures were then derived to include temporal changes within a SS, the LOBULAR components each COMPOUND encountered plus the path each COMPOUND traversed, the length of each traversed path, and each COMPOUND'S resident time within an ISL or one of its features.

During the first phase, two types of raw tracing data were generated. A trace data file was generated for each SS including PV and CV. It recorded the temporal order of events experienced by all COMPOUNDS that resided within a particular SS. To trace METABOLIC events, each SS NODE also generated a tracing file that listed the COMPOUND'S identification and type along with the TIME METABOLISM occurred.

Collected data were evaluated during phase two. The tracing process and steps within are diagrammed in Supplementary Fig. S2 online. We started by tracing changes at Levels 1 and 2 (Fig. 2): changes associated with ENDOTHELIAL CELLS, HEPATOCYTES, ENZYMES, and BINDERS at level 1 and within the four SS spaces. Tracing results at higher levels were deduced by aggregating results from lower levels. A traverse path provided an image of each SS node visited by a COMPOUND during its course through a LOBULE. Not all injected COMPOUNDS reached the CV. Some were METABOLIZED. Others were retained because of multiple binding events. All paths started at PV; they ended at either CV or with the SS where the COMPOUND was METABOLIZED or remained when the run terminated. Traverse length summed the length of each SS entered. The fine-grain paths taken by a COMPOUND within Levels 5 and 6 were ignored. Regardless of path taken by a COMPOUND within a SS, its traverse length was simply the length (in grid spaces) of that SS. Residence time was the TIME spent within the ISL before exiting, being METABOLIZED, or having the run terminate. Each component that encountered a COMPOUND recorded the number and type of COMPOUND with which it interacted.

JPET Fast Forward. Published on April 20, 2010 as DOI: 10.1124/jpet.110.168526
This article has not been copyedited and formatted. The final version may differ from this version.

Results

Initial iterative ISL refinement. We sought outflow profiles produced by NORMAL and two types of DISEASED ISLs, derived from that NORMAL ISL, that would achieve SM > 0.9. We named the latter two $DISEASED_{CCl4}$ and $DISEASED_{ALC}$. Absent evidence that major features of lobular anatomy (zonation, primary flow paths and their arrangement) were meaningfully different between the three liver types, we specified that in the ISLs they would be essentially the same. Earlier (Park et al., 2009), we described a $DISEASED_{CCl4}$ ISL that validated against a diltiazem outflow profile from a diseased, CCl_4-treated liver. It was achieved by adjusting ten parameters of a NORMAL ISL that had validated against a diltiazem outflow profile from a normal liver. Adhering to the parsimony guideline, we sought an alternative parameterization (limited to the same ten parameters) of that NORMAL ISL that would also produce a $DISEASED_{ALC}$ ISL that could achieve SM > 0.9. We sampled ISL parameter space many times and found alternative NORMAL ISLs that could be transformed to either a $DISEASED_{CCl4}$ or $DISEASED_{ALC}$ ISL (for which a SM > 0.9 could be achieved), but not both. That failure falsified that earlier, NORMAL ISL as a starting model for achieving both $DISEASED_{CCl4}$ and $DISEASED_{ALC}$ ISLs. An alternative, validated NORMAL ISL was needed. Note, however, that earlier, NORMAL ISL remained valid when outflow profiles from only normal and CCl_4-treated livers were targeted. Again, adhering to the parsimony guideline, we increased the number of parameters available to adjust from ten to eleven and subsequently to the twelve, which proved adequate. The two additional parameters that were available for adjustment were ENDOTHELIAL CELL density (*ECDensity*) and *SinusoidTurbo*, which biases COMPOUND random walk in the direction of the CV.

Validation of disposition in NORMAL and DISEASED ISLs. As described in Methods, we specified that achieving SM > 0.9 within a factor of 0.33 of referent data was an acceptable target: an outflow profile that meets that SM was accepted as being experimentally indistinguishable from its referent profile. Through use of the new parameter sweeping capability (Supplementary Fig. S1 online), we iteratively adjusted the new NORMAL ISL parameter values (Table 1) to move outflow profile properties toward those of diltiazem and sucrose from CCl_4-treated livers. We continued that process until the outflow profile achieved SM > 0.9. We then repeated that protocol with outflow profiles from an alcohol-treated liver to obtain validated $DISEASED_{ALC}$ ISLs. Parameter adjustments that enabled achieving SM > 0.9 are diagrammed in Fig. 4. DILTIAZEM outflow profiles from each of the three ISLs are graphed in Fig. 3. SM values for unsmoothed profiles were 0.92 (NORMAL), 0.92 ($DISEASED_{CCl4}$), and 0.91 ($DISEASED_{ALC}$).

JPET Fast Forward. Published on April 20, 2010 as DOI: 10.1124/jpet.110.168526
This article has not been copyedited and formatted. The final version may differ from this version.

The ISL is nonlinear. Consequently, linear sensitivity studies are less informative and less meaningful than are location changes in LOBULE parameter space. Individually, the parameter changes in Fig. 4 did not cause statistically distinguishable changes in outflow profiles. In general, a 5% change in any one of the twelve adjusted parameters will produce an imperceptible change in an outflow profile and no change in SM value. However, a 5% change in all twelve parameters can cause a noticeable change in outflow profile.

Note that the $\text{DISEASED}_{\text{ALC}}$ ISL was simpler than the $\text{DISEASED}_{\text{CCl4}}$ ISL in two ways. 1) Whereas twelve lobular parameter adjustments were needed to achieve $\text{DISEASED}_{\text{CCl4}}$ ISLs, only six were needed to achieve $\text{DISEASED}_{\text{ALC}}$ ISLs. 2) Except for the *C2BJumpProb* adjustments, the magnitude of the adjustments needed for $\text{DISEASED}_{\text{ALC}}$ ISL was smaller than those of $\text{DISEASED}_{\text{CCl4}}$ ISL. The fact that $\text{DISEASED}_{\text{ALC}}$ ISLs exhibit fewer, smaller magnitude changes relative to NORMAL ISLs is consistent with less profound and fewer observed pathological changes caused by alcohol pretreatment (Hung et al., 2002a,b).

Hereafter, all results are reported in the order NORMAL, $\text{DISEASED}_{\text{CCl4}}$ and, $\text{DISEASED}_{\text{ALC}}$, when values for all three are provided, and in the order $\text{DISEASED}_{\text{CCl4}}$ and $\text{DISEASED}_{\text{ALC}}$ when only DISEASED ISL values are provided.

Changes in LOBULE properties at three levels can account for CIRRHOSIS-caused differences in disposition. CELL density in Spaces B and C were controlled by *ECDensity* and *HepDensity*. The value of *ECDensity* (0.65) was unchanged for $\text{DISEASED}_{\text{ALC}}$ ISLs, but was smaller (0.6) for $\text{DISEASED}_{\text{CCl4}}$ ISLs. The values of *HepDensity* reflect the same change: 0.7, 0.65, and 0.7 (Fig. 4). The latter difference maps to the observed, CCl_4-induced changes in hepatocyte quantitative ultrastructure (Hung et al., 2002b). Acceptable SM values were obtained without having to change the probability that a DILTIAZEM released from an ENZYME (in HEPATOCYTES) would be a METABOLITE.

Four parameters control COMPOUND movement between Spaces (Fig. 4, top row). Lower values relative to NORMAL for the first two mean that DISEASE reduced COMPOUND access to ENDOTHELIAL CELLS and HEPATOCYTES. The magnitude and direction of those changes map to and are consistent with fibrotic changes (Hung et al., 2002a). The effective ability of Space C to retain COMPOUNDS (*B2CJumpProb/C2BJumpProb*) is a major determinant of the METABOLIC event rate. That ratio in $\text{DISEASED}_{\text{ALC}}$ ISLs (2.6) was larger than that in NORMAL (1.2) or $\text{DISEASED}_{\text{CCl4}}$ (0.62) ISLs. The larger ratio reduced the total number of DILTIAZEMS reaching CV thereby increasing METABOLIC events within Space C. *HepDensity's* value was smaller in $\text{DISEASED}_{\text{CCl4}}$ (0.65) than in NORMAL or $\text{DISEASED}_{\text{ALC}}$ (0.70) ISLs, and

JPET Fast Forward. Published on April 20, 2010 as DOI: 10.1124/jpet.110.168526
This article has not been copyedited and formatted. The final version may differ from this version.

that contributed to decreased METABOLIC events and diminished DILTIAZEM retention in Space C.

The graphs in Fig. 5A,B show how stochastic COMPOUND movements within the three spaces influenced average COMPOUND resident TIMES within LOBULES. The bar graphs specify the DOSE fraction having resident TIMES within the indicated ten-SECOND range. The three curves specify the fraction of dose having a LOBULE resident TIME equal to or less than the indicated TIME. SUCROSE (Fig. 5A) did not enter CELLS. The bar graphs (a.1 and a.2) indicate that there were few differences in the spaces accessed and dwelt in by SUCROSE in NORMAL and $DISEASED_{ALC}$ ISLs. However, SUCROSES dwell TIMES in the $DISEASED_{CCl4}$ ISLs were different in two ways. There was a dramatic reduction in SUCROSES having longer and also 0–10 SECOND dwell TIMES.

Dwell TIME patterns were quite different for DILTIAZEM (Fig. 5B). For both DISEASED ISLs, there was a reduction in DILTIAZEMS having 0–10 SECOND dwell TIMES, and an increase in DILTIAZEMS having 10–20 SECOND dwell TIMES. The net effect was an increase in DILTIAZEMS having longer dwell TIMES: disease makes it harder for diltiazem to move through and exit a diseased liver. DISEASE type altered dwell TIME patterns differently (b.2 and b.3). Surprisingly, there were no significant differences in mean (and SD) DILTIAZEM resident TIMES: 47.8 (26.0), 48.8 (25.2), and 45.9 (26.5) SECONDS. Several factors influenced the differences between resident TIMES. Differences in *A2BJumpProb* between the three ISL types (0.38, 0.21, and 0.35) caused fewer DILTIAZEMS to move into Space B in DISEASED relative to NORMAL LOBULES. Similarly, differences in *B2CJumpProb* (0.55, 0.34, and 0.65) caused fewer of the DILTIAZEMS that did reach Space B in $DISEASED_{CCl4}$ relative to $DISEASED_{ALC}$ to move on to Space C.

Changes in dwell TIME patterns coupled with changes in access to Spaces A–C influence METABOLISM appreciably. The fraction of dose that was METABOLIZED (that underwent a METABOLIC event) by a given TIME is graphed in Fig. 5C.

Tracing COMPOUND path lengths and spatiotemporal binding patterns. The path length curves in Fig. 6A,B measure cumulative lengths of all SSs entered by each COMPOUND. All three ISL types had 70 SSs distributed among the three zones. A small subset of both DILTIAZEM and SUCROSE path lengths in NORMAL and $DISEASED_{ALC}$ ISLs were long (second peak in Fig. 6A,B), but they were essentially absent in the DISEASED ISLs. The SSs in Zone 1, in combination with intra-zone edges map to the interconnections between sinusoids that are most numerous in the periportal region, yet are absent in the perivenous region of

JPET Fast Forward. Published on April 20, 2010 as DOI: 10.1124/jpet.110.168526
This article has not been copyedited and formatted. The final version may differ from this version.

normal lobules. Microscopy evidence suggests that some of those interconnections are lost in CCl_4-treated, cirrhotic lobules (Gaudio and Onori, 1997).

There are no wet-lab methods to measure which lobular subspaces are visited by a compound passing through the liver. We recorded each COMPOUND'S traverse path (in grid spaces) for 100 SECONDS, until it either exited the LOBULE, was METABOLIZED, or the run ended. SUCROSE had shorter path lengths because it did not enter CELLS and so was more likely to reach CV before the run terminated. The shorter mean path for DISEASED ISLs shows that both DISEASE types made it easier for COMPOUNDS to move closer to CV as TIME advanced. It is evident from Fig. 6A,B inserts that $DISEASED_{CCl4}$ ISLs had a more narrowly distributed variety of path lengths. Note also that the $DISEASED_{CCl4}$ ISLs had fewer of the shortest paths (0–25 grid spaces) than either NORMAL or $DISEASED_{ALC}$ ISLs.

Each component type that encountered and interacted with DILTIAZEMS and SUCROSE was recorded. The TIME DILTIAZEMS spent associated with components was in the order ENZYMES > BINDERS > (unbound in) HEPATOCYTES > (unbound in) ENDOTHELIAL CELLS. For all components, influential factors included the population density of DILTIAZEMS in each space, traverse lengths, and the values of these three parameters in Fig. 4: *SoluteBindingProb*, *SoluteBindingCycles*, and *BindersPerCell*. Despite those differences, the data in Fig. 6C,D show that the fraction of COMPOUNDS that was in a LOBULE at a particular TIME and attached to a BINDER eventually reached a similar steady state ratio of about 0.8 in $DISEASED_{CCl4}$ and $DISEASED_{ALC}$ LOBULES. However, the relative fractions BOUND in ENDOTHELIAL (Space B) and HEPATOCYTE layers (Space C) were different.

COMPOUND dynamics within and between zones. Observing DILTIAZEMS percolating through individual SS within different zones provides an informative perspective. A video recording of COMPOUNDS percolating through SSs in an earlier ISL is provided as a Supplement by Yan et al. (2008a) Selected results are graphed in Fig. 7 and Supplementary Fig. S3 online for one similar sized SS in each of the three zones. Figure 7 shows the fraction of DILTIAZEM dose within Core and Spaces A–C of the selected SS, regardless DILTIAZEM'S state or location. The differences in relative trends between zones are striking. Zone 2 peaks occur later than those in Zone 1. The amount of DILTIAZEM trickling through Zone 3 was still increasing at 40 SECONDS for all three ISLs. The relative patterns for NORMAL and $DISEASED_{ALC}$ SS within the same zone are similar and clearly different from those in the $DISEASED_{CCl4}$ SS. More DILTIAZEM was in Spaces A and B of all three $DISEASED_{CCl4}$ SS compared to NORMAL and $DISEASED_{ALC}$ SS, and that may map to fibrosis

JPET Fast Forward. Published on April 20, 2010 as DOI: 10.1124/jpet.110.168526
This article has not been copyedited and formatted. The final version may differ from this version.

retarding diltiazem's access to spaces more distant from blood flow.

A portion of the data in Fig. 7 is shown subdivided further in Supplementary Fig. S1 online into bound and unbound DILTIAZEM within the ENDOTHELIAL and HEPATOCYTE layers (Spaces B and C). The dramatic increase in the binding of DILTIAZEM within ENDOTHELIAL layers (keeping it away from the HEPATOCYTE layer) maps to the observed fibrotic changes.

Discussion

Tracing multiscale events facilitated identifying plausible micromechanistic differences regarding where and how NORMAL and DISEASED ISLs interacted differently with DILTIAZEM and SUCROSE. It is currently infeasible to obtain comparable wet-lab data, but advances in intravital microscopy methods are moving us closer. The outflow profiles in Fig. 3 achieved a degree of validation against wet-lab counterparts. That achievement allows us to conjecture that mappings exists between micromechanistic causes determining DILTIAZEM disposition in the three types of ISLs (mappings 1 and 2 in Fig. 1) and corresponding causes in normal and diseased perfused livers. DILTIAZEM and SUCROSE dynamics within and between ISL levels provide heretofore-unavailable insight into plausible disposition details. However, the ISLs are not yet sufficiently refined to make precise predictions. With additional rounds of refinement and validation, their progeny can be expected to provide increasingly useful scientific predictions, as well as deeper insight into causal micromechanisms.

Similarity was achieved without having to use different NORMAL and DISEASED SINUSOID networks. However, it is premature to assign biological significance to that lack of difference. The three ISLs are specific examples of a number of similar ISLs that would also validate (analogous to how livers from matched rats are different, but for experimental purposes can be treated as being the same). To emphasize that we are early on the path to strong validation and trust, we have confined our rhetoric to describing and contrasting what occurred during ISL executions, and have drawn attention when those phenomena were consistent (or not) with reported wet-lab observations. Additional, more detailed observations on results are included in Supplementary Material.

The take-home message has five parts. 1) Multilevel ISL changes provide plausible mechanistic explanations for differences in compound disposition between normal and diseased livers. 2) LOBULES changed at three levels: SS geometry; CELL density and COMPOUND movement between SS spaces; and

JPET Fast Forward. Published on April 20, 2010 as DOI: 10.1124/jpet.110.168526
This article has not been copyedited and formatted. The final version may differ from this version.

INTRACELLULAR processes. 3) As illustrated in Fig. 8, those changes may have counterparts during disease progression. Twelve (of 29) ISL parameters were involved in NORMAL-to-DISEASED$_{CCl4}$ translation. However, six of those were invariant for NORMAL-to-DISEASED$_{ALC}$ translation. 4) Counterintuitively, three of the parameter changes required for translation changed in *opposite* directions. 5) Tracings of micromechanistic events *below the validation level* were required for a meaningful discussion of the results. So doing increased the heuristic value of ISL models.

All of the wet-lab data in Fig. 4 are coarse-grained, end-of-experiment, whole liver measures. Each ISL parameter, on the other hand, influences fine-grained, spatiotemporal events occurring during simulation. Consequently, the two sets of data are not easily compared. For convenience, descriptions of all measures, along with conjectures on how ISL parameter values may relate to them, are provided under Supplementary Discussion in Supplementary Material. None of the wet-lab measures in Fig. 4 were included as targeted attributes. There were two reasons. 1) We do not know if or how the phenomena measured might actually influence the disposition of diltiazem or sucrose. 2) With the exception of extent of DILTIAZEM METABOLISM, which can map to intrinsic clearance and CYP450, there were no measurable ISL features that map logically to the other six histopathology measures. Nevertheless, neither the wet-lab data in Fig. 4 nor other histopathology data reported in the original citations (Hung et al., 2002a,b) falsify any ISL parameter changes in Fig. 4.

ISL METABOLIC events map to intrinsic clearance. The ratio of METABOLIC events in Fig. 5 for DISEASED and NORMAL ISLs maps to differences in intrinsic clearance for the different livers. No ISL parameter maps to CYP450. *BindersPerCell* does not; it maps to all cellular material that binds or sequesters diltiazem including the metabolizing enzymes. However, it is not surprising that wet-lab CYP450 and intrinsic clearance changes correlate. We can thus say that the ratio of METABOLIC events in DISEASED to NORMAL ISL also maps to CYP450 changes. Because DISEASED ISL parameterizations were iteratively refined starting from the NORMAL ISL, without regard to metabolism, the METABOLISM data in Fig. 5 can be taken as predictions that validated.

Assume that future data shows that sinusoid networks are different between normal and diseased livers in specific ways. Inclusion of that data in the targeted attribute list would invalidate the current DISEASED ISLs. However, it would be straightforward to iteratively revise them until validation is again achieved. It is even feasible to automate that process.

JPET Fast Forward. Published on April 20, 2010 as DOI: 10.1124/jpet.110.168526
This article has not been copyedited and formatted. The final version may differ from this version.

Deep tracing of the type presented in Figs. 5-7 can present methodological challenges and problems because synthetic models are designed to realize an explicit separation between generators (micromechanisms) and phenomena. ISLs are completely observable, unlike livers. An asset is the ability to reach into the ISL and watch everything that happens. Doing so, however, may bias a researcher into trusting an ISL more than is warranted. For example, the ISL is relatively grounded in terms of runs, cycles, and steps of its various macro-, meso-, and micro-constituents. The referent data against which we validated requires a very coarse measure, the outflow fraction profile. Hence, any measures, like the tracings in Figs. 5–7 that are finer-grained, although clearly relevant to the ISL, may not be valid in relation to the referent. It remains an untested hypothesis because we do not have data against which to validate.

The SS graph is not explicitly spatial. It is an abstract network of SS nodes that have no concrete mapping to the spatial structure of sinusoids within referent liver lobules. However, in aggregate it performs enough like a lobule to produce matching outflow profiles: quantifiable mappings from ISL to referent traverse paths may exist. Because outflow profiles are our validation data, there is no need to make LOBULES explicitly spatial. Adding such a requirement merely for the purpose of making the structure of the LOBULE more intuitive or "more like" the referent, absent any fine-grained spatial data against which to validate, runs counter to the parsimony guideline. There is some reasonable pressure to make the lobule spatially explicit, however. Lobular zonation data exists (e.g., Gebhardt, 1992; Jungerman, 1995; Oinonen and Lindros, 1998; Christoffels, et al., 1999; Ohno et al., 2008) and is explicitly spatial. Because current LOBULES can contain graphs that cannot be projected onto a 3D vector space, validation against such zonation data is difficult. Doing so would be more straightforward if the ISL lobules were spatially explicit. We are exploring strategies for making them so for future experiments.

We suggest that the incremental parameter changes that are necessary (and sufficient) to transform a NORMAL into a DISEASED ISL (the changes on the right side of Fig. 1) may correspond abstractly to molecular, cellular, and sinusoid level transformations responsible for the pathogenesis from normal into diseased livers during CCl_4 and alcohol treatment as illustrated in Fig. 8. The general consistency noted above between DISEASED ISLs during execution and the cited histopathology evidence supports the hypothesis. We thus have a tentative, yet promising, in silico model that enables us to visualize, abstractly from the perspective of diltiazem, how the consequences of cirrhosis may have progressed. That new capability represents an important step toward unraveling the complex influences of disease on drug

disposition. Being able to transform one validated model into another is also important: it is evidence that the approach can facilitate rational translation of research results to useful applications, and that may open doors to development of strategies for tailoring drug choices to help reverse disease conditions.

Having independently validated NORMAL and DISEASED ISLs allows one to explore plausible drug disposition consequences of intermediate levels of disease and even disease that is more advanced. Because of individual differences in disease progression, conducting wet-lab experiments to document the former would be problematic, and the latter may be deemed unethical. By assuming disease progression corresponds to gradual change from NORMAL to DISEASED ISL parameterizations, we can simulate a liver that has progressed half way, for example, along the path to the currently documented disease state. We can project further parameter changes to explore plausible consequences of more advanced level of disease. Corresponding explorations of intermediate and advanced disease states would be infeasible using traditional inductive, physiologically based, mathematical models.

The methods and approach have been designed to enable the eventual development of horizontally and vertically integrated whole organism—whole patient—analogues: virtual organs, virtual patients. Once that goal has been achieved, it will be feasible prior to treatment to use in silico experimentation to anticipate narrow, plausible ranges of drug PK properties in patients with liver disease.

Acknowledgements

We thank members of the BioSystems Group for helpful discussion and commentary. SP and SHJK developed and implemented tracing methods. CAH and GEPR designed and GEPR implemented and verified the ISL. CAH designed experiments. SP and SHJK conducted experiments and analyzed results. CAH developed and finalized the manuscript and figures using contributions from SP, GEPR, and SHJK. CAH, GEPR, SHJK, and SP edited and revised the manuscript. MSR proved the wet-lab data and editing suggestions. This work was supported by CDH Research Foundation (SP and SHJK) [Grants CDHRP-06/07, -0014, -0023]; and by Australian National Health and Medical Research Council (MSR) [Grant 252871/9937600].

JPET Fast Forward. Published on April 20, 2010 as DOI: 10.1124/jpet.110.168526
This article has not been copyedited and formatted. The final version may differ from this version.

References

Christoffels VM, Sassi H, Ruijter JM, Moorman AF, Grange T, and Lamers WH (1999) A mechanistic model for the development and maintenance of portocentral gradients in gene expression in the liver. *Hepatology* **29**: 1180-92.

Dourakis SP (2008) Drug therapy in liver disease. *Ann Gastroent* **21**: 215-217.

Fisher J and Henzinger TA (2007) Executable cell biology. *Nat Biotech* **25**: 1239-49.

Gaudio E, Onori P, Franchitto A, Sferra R, and Riggio O (1997) Liver Metabolic Zonation and Hepatic Microcirculation in Carbon Tetrachloride-Induced Experimental Cirrhosis. *Diges Dis Sci* **42**: 167-77.

Gebhardt R (1992) Metabolic zonation of the liver: Regulation and implications for liver function. *Pharmacol Ther* **53**: 275-354.

Gumucio JJ, and Miller DL (1982) Zonal hepatic function: solute-hepatocyte interactions within the liver acinus. *Prog Liver Diseases* **7**: 17–30.

Hung DY, Chang P, Weiss M, and Roberts MS (2001) Structure-hepatic disposition relationships for cationic drugs in isolated physiological models. *J Pharmacol Exp Ther* **297**: 780-9.

Hung DY, Chang P, Cheung K, McWhinney B, Masci PP, Weiss M, and Roberts MS (2002a) Cationic drug pharmacokinetics in diseased livers determined by fibrosis index, hepatic protein content, microsomal activity, and nature of drug. *J Pharmacol Exp Ther* **301**: 1079-87.

Hung DY, Chang P, Cheung K, Winterford C, and Roberts MS (2002b) Quantitative evaluation of altered hepatic spaces and membrane transport in fibrotic rat liver. *Hepatology* **36**: 1180-89.

Hunt CA, Ropella GEP, Yan L, Hung DY and Roberts MS (2006) Physiologically based synthetic models of hepatic disposition. *J Pharmacokinet Pharmacodyn* **33**: 737-72.

Hunt CA, Ropella GEP, Park S, and Jesse Engelberg J (2008) The Real Dichotomies Between Computational and Mathematical Models. *Nat Biotech* **26**: 737-738.

Hunt CA, Ropella GE, Lam TN, Tang J, Kim SH, Engelberg J, and S. Sheikh-Bahaei S (2009) At the Biological Modeling and Simulation Frontier. *Pharm Res* **26**: 2369-2400.

Jungermann K (1995) Zonation of metabolism and gene expression in liver. *Histochem Cell Biol* **103**: 81-91.

Le Couteur DG, Fraser R, Hilmer S, Rivory LP, and McLean AJ (2005) The hepatic sinusoid in aging and

cirrhosis: effects on hepatic substrate disposition and drug clearance. *Clin Pharmacokinet* **44**: 187-200.

Liu L and Pang KS (2007) An integrated approach to model hepatic drug clearance. *Eur J Pharm Sci* **29**: 215–23.

Mager DE and Jusko WJ (2006) Quantitative structure-pharmacokinetic/pharmacodynamic relationships. *Adv Drug Del Rev* **58**: 1326–1356.

Miller DL, Zanolli CS, and Gumucio JJ (1979) Quantitative morphology of the sinusoids of the hepatic acinus. Quantimet analysis of rat liver. *Gastroenterol* **76**: 965–969.

Ohno H, Naito Y, Nakajima H, and Tomita M (2008) Construction of a biological tissue model based on a single-cell model: a computer simulation of metabolic heterogeneity in the liver lobule. *Artif Life* **14**: 3-28.

Oinonen T and Lindros KO (1998) Zonation of hepatic cytochrome P-450 expression and regulation. *Biochem J* **329**: 17-35.

Park S, Ropella GE, Kim SH, Roberts MS, and Hunt CA (2009) Computational strategies unravel and trace how liver disease changes hepatic drug disposition. *J Pharmaco Exp Ther* **328**: 294-305.

Rescigno A (2004) On the use of pharmacokinetic models. *Phys Med Biol* **49**: 4657–4676.

Ropella GE, Nag DA, and Hunt CA (2003) Similarity measures for automated comparison of in silico and in vitro experimental results. *Proceedings of the 25th Annual International Conference of the IEEE Engineering in Medicine and Biology Society* **2** (April 17–21): 2933–2936 (ISBN: 0-7803-7789-3).

Siebert GA, DY. Hung, P. Chang, and MS. Roberts. Ion-trapping, microsomal binding, and unbound drug distribution in the hepatic retention of basic drugs. *J Pharmacol Exp Ther* 308:228–235, 2004.

Yan L, Ropella GEP, Park S, Roberts MS, and Hunt CA (2008a) Modeling and simulation of hepatic drug disposition using a physiologically based, multi-agent in silico liver. *Pharm Res* **25**: 1023-36.

Yan L, Sheihk-Bahaei S, Park S, Ropella GEP, and Hunt CA (2008b) Predictions of hepatic disposition properties using a mechanistically realistic, physiologically based model. *Drug Metab Dispos* **36**: 759-68.

Yan L, Park S, Sheihk-Bahaei S, Ropella GEP, and Hunt CA (2008c) Predicting hepatic disposition properties of cationic drugs using a physiologically based, agent-oriented In Silico Liver. *Proceedings of the 2008 Agent-Directed Simulation Symposium* (Yilmaz L, et al. eds); 2008 April 14-16; Ottawa, ON, pp. 162-69, SCS Press, San Diego, CA (ISBN: 1-56555-319-5).

Footnote

This work was supported by CDH Research Foundation (SP and SHJK) [Grants CDHRP-06/07, -0014, -0023]; and by Australian National Health and Medical Research Council (MSR) [Grant 252871/9937600].

JPET Fast Forward. Published on April 20, 2010 as DOI: 10.1124/jpet.110.168526
This article has not been copyedited and formatted. The final version may differ from this version.

Legends to Figures

Figure 1. Shown are relationships between the wet-lab perfused liver models and different computational models. **a**: During experiments, liver components in their experimental context interact with transiting drug molecules causing changes in the compound's concentration-time profile. Systemic behaviors at all levels are reflected in the data. **b**: Illustrated is an induced PK model of data from (a). The researcher identifies patterns in the data. A mechanistic description is induced, having an abstract, conceptual mapping from that description to hepatic disposition mechanisms. A set of PK equations is offered to describe patterns in the data. A discretized model of the equations in software is constructed and executed to simulate parameterized equation output. Metrics specify the goodness of fit, establishing a concrete mapping from simulated output to wet-lab data. **c**: The mechanism and component descriptions (quantitative and qualitative) are knowledge-based. Abstract, software components are designed, coded, verified, assembled, and connected guided by that mechanistic description. The product of the process is a NORMAL LOBULE (Fig. 2). Concretizable mapping 1 exists between LOBULE components and how they plug together, and hepatic physiological and microanatomic details. Compilation and source code execution gives rise to a working analogue; measures of events give the traced results. Dynamics during execution (mapping 2) are intended to represent abstractly plausible corresponding dynamics (believed to occur) within the liver during an experiment. Mapping 2 can also be concretized iteratively. Measures of dynamics provide data intended to mimic counterpart measures. Achieving measurable similarities makes mapping 3 quantitative. **d**: DISEASED counterparts to NORMAL ISLs: simple adjustments (increase or decrease) covert a subset of NORMAL parameter values, mechanisms, and events into DISEASED counterparts that validate. **e**: The equations from (b) are used to fit PK data from perfusion experiments on diseased livers (Hung et al., 2002a), and disease specific PK parameter values are obtained. Conceptual mappings are offered to relate differences in parameter values (NORMAL to DISEASED and $\text{DISEASED}_{\text{CCl4}}$ to $\text{DISEASED}_{\text{ALC}}$) to measures of histopathology. However (∗), because those conceptual mappings cannot be concretized, they cannot be verified or validated. The parameterized equations, however, can be validated based on the quality of their fit to the temporal outflow profiles.

Figure 2. Multilevel structure of an In Silico Liver (ISL). See text for details. A LOBULE maps to the functional unit of the liver, which consists of portal vein tracts (PV), a central vein (CV), and interconnected sinusoids. Flow is PV → CV. There are three zones. A LOBULE network is specified using an inter-

JPET Fast Forward. Published on April 20, 2010 as DOI: 10.1124/jpet.110.168526
This article has not been copyedited and formatted. The final version may differ from this version.

connected directed graph having 70 nodes organized into three zones. Intra-zonal connections are possible. Three types of inter-zone connections are used: Zone 1 → Zone 2, Zone 1 → Zone 3, and Zone 2 → Zone 3. A Sinusoidal Segment (SS) maps to a unit sinusoid structure and function. One SS is placed at each graph node. It contains a Core and three two-dimensional toroidal grid spaces. Space A maps to the interface between blood flow and cells. Space B is called the ENDOTHELIAL layer; it contains ENDOTHELIAL CELLS and EXTRACELLULAR spaces; ENDOTHELIAL CELLS contain BINDERS. Space C is called the HEPATOCYTE layer; it contains HEPATOCYTES and EXTRACELLULAR spaces; HEPATOCYTES contain BINDERS that function as DILTIAZEM METABOLIZING ENZYMES. Objects representing diltiazem and sucrose move within and between spaces; DILTIAZEM can move in and out of CELLS.

Figure 3. Outflow profiles of DILTIAZEM in NORMAL and DISEASED ISLs. Smoothed DILTIAZEM outflow profiles are plotted for NORMAL **(A)**, $\text{DISEASED}_{\text{CCl4}}$ **(B)**, and $\text{DISEASED}_{\text{ALC}}$ **(C)** ISLs. They achieved validation by having SM > 0.9. An example of raw, unsmoothed data is shown in (B). ISL data are averages of 48 runs (performed in Experiment Level Parallel mode) using 48 variants of a LOBULE having a specified graph structure; the parameter vector for each of the 48 LOBULES is Monte Carlo specified. Solid lines connecting referent perfused liver outflow data are graphed along with the output of the fitted PK model (dotted curves) (Hung et al, 2002b); see Supplementary Material for details of the PK models. In each experiment, equal numbers of DILTIAZEM and SUCROSE were co-administered using the dosing function parameterized as specified in Table 1. Parameter sweeping was used to discover for a parameter vector that would produce SM > 0.8. That profile was refined and improved iteratively in Experiment Level Parallel mode until SM > 0.9.

Figure 4. Properties of ISLs and experimental livers. Top: Parameter values are graphed for NORMAL and DISEASED ISLs. Parameter descriptions are provided in the Appendix. Top row: These parameters control probabilistic movement of DILTIAZEM and SUCROSE between the four SS spaces (Fig. 2). Bottom (Wet-Lab): Tissue pathology measures (Hung et al., 2002a) taken at the end of the perfusion are graphed for whole normal and diseased livers. None of these measures were targeted attributes. Measures of CCl_4 and alcohol treated livers had separate control values. To facilitate comparisons, the values graphed are normalized to corresponding control values. Intrinsic clearance is for diltiazem. CYP-450 (a measure of all isozymes), microsomal protein, and cytoskeleton residue are biochemical measures. Membrane thickness and number of fenestrae are from microscopic observations. Permeability (ability of water to permeate hepatic tissue) and

JPET Fast Forward. Published on April 20, 2010 as DOI: 10.1124/jpet.110.168526
This article has not been copyedited and formatted. The final version may differ from this version.

albumin space are derived measures from liver perfusion experiments. Additional detail is provided in Supplementary Material.

Figure 5. Results from tracing COMPOUND resident TIMES and DILTIAZEM METABOLIC events within an average LOBULE. **A**, **B**: Each curve is the cumulative sum of bar heights from one of a.1–a.3, b.1–b.3, which are average LOBULE resident TIME histograms for SUCROSE (A) and DILTIAZEM (B): the average amount of TIME a COMPOUND resided in a LOBULE was measured. A point on each curve designates the dose fraction that had resident TIME ≤ the indicated TIME. Each COMPOUND was traced from initial injection until it was METABOLIZED, cleared from the LOBULE through the CV, or the run ended. Bar heights measure the fraction of dose having resident TIMES within the indicated ten-SECOND interval. **C**: The TIME of a METABOLIC event was recorded. The curves are the cumulative fraction of DILTIAZEM dose that was METABOLIZED by the indicated TIME.

Figure 6. Results from tracing COMPOUND traverse path lengths and DILTIAZEM binding. **A**: Traverse path lengths of DILTIAZEM: each curve is the cumulative sum of bar heights from one of a.1–a.3. Each traverse length is the sum of the lengths (in grid spaces) of each SS visited by a DILTIAZEM prior to collection at the CV, being METABOLIZED, or the run's end. COMPOUND wandering within SS was ignored. Histogram bin size is 25 grid spaces. Bar height corresponds to fraction of administered COMPOUND. **B**: Data for coadministered SUCROSE, measured and graphed the same as in (A). **C**, **D**: Data are fraction of DILTIAZEM dose bound at intervals during simulation experiments that used $\text{DISEASED}_{\text{CCl4}}$ ISLs (C) and $\text{DISEASED}_{\text{ALC}}$ ISLs (D).

Figure 7. Fraction of DILTIAZEM dose within different SS spaces in each zone. A comparable size SS was selected from Zone 1 (three left panels), Zone 2 (three center panels), and Zone 3 (three right panels) from a NORMAL (three top panels), a $\text{DISEASED}_{\text{ALC}}$ (three middle panels), and a $\text{DISEASED}_{\text{CCl4}}$ ISL (three bottom panels). In each panel, the dose fraction (regardless of location or state) at indicated times is plotted for Core and Spaces A–C. The curves are approximate trend lines. The bumps in several are the result of a "wave" of compound entering this SS from an upstream SS. Such variability tends to cancel out as results over many SS are summed.

Figure 8. Relationships among models and their transformations are illustrated. Validation establishes clear, concretizable mappings from NORMAL ISLs during simulations to normal liver counterparts during perfusion experiments. We can hypothesize that similar mappings exist between validated DISEASED ISLs

JPET Fast Forward. Published on April 20, 2010 as DOI: 10.1124/jpet.110.168526
This article has not been copyedited and formatted. The final version may differ from this version.

and wet-lab counterparts. Left: Upon validation for the attributes targeted, we can use intermediate parameterizations to document the incremental transformation of a NORMAL to a DISEASED ISL. The details of such an in silico transformation provide a working, abstract hypothesis for the mechanisms of actual disease progression from the perspective of diltiazem.

JPET Fast Forward. Published on April 20, 2010 as DOI: 10.1124/jpet.110.168526
This article has not been copyedited and formatted. The final version may differ from this version.

Table

Table 1. NORMAL and DISEASED ISL parameters. Values were obtained following validation against the profile of diltiazem co-administered with sucrose. Parameters marked (•) were different for NORMAL and DISEASED ISLs. Parameters marked (§) are sensitive to differences in COMPOUND physicochemical properties.

Parameter Group	Parameter	Normal	Diseased$_{CCl4}$	Diseased$_{ALC}$	Description
Simulation Execution and Evaluation	*monteCarloRuns*	48	48	48	Simulation Control
	cycleLimit	200	200	200	
	stepsPerCycle	2	2	2	
	currentRuns	0	0	0	
	runFileNameBase	run	run	run	Simulation Monitor
	nominalProfile	dat	dat	dat	
	SimularityMeasure	global_sd	global_sd	global_sd	Result Evaluation
LOBULE	*GraphInputFile*				
	GraphSpecFile	lobule-j301	lobule-j301	lobule-j301	SINUSOIDAL Network
	GraphSpecIterates	1	1	1	
	• *SSTypeRatio*	19	99	19	Shorter, wider SS Specification
	• *DirSinCirc*	24	22	24	
	DirSinLenAlpha	1.0	1.0	1.0	
	DirSinLenBeta	0.085	0.085	0.085	
	DirSinLenShift	3.0	3.0	3.0	
	TortSinCirc	3	3	3	Longer, thinner SS Specification
	TortSinLenAlpha	12.0	12.0	12.0	
	TortSinLenBeta	0.075	0.075	0.075	
	• *A2BJumpProb* §	0.38	0.20	0.35	Probabilistic COMPOUND Movement
	• *B2AJumpProb* §	0.37	0.30	0.35	
	• *B2CJumpProb* §	0.55	0.34	0.65	
	• *C2BJumpProb* §	0.478	0.55	0.25	
	CoreFlowRate	2	2	2	FLOW RATE Control
	• *SinusoidTurbo*	0.82	0.85	0.82	
	• *ECDensity*	0.65	0.60	0.65	CELL Density
	• *HepDensity*	0.70	0.65	0.70	
	• *BindersPerCell* §	95	65	75	SOLUTE BINDING Control
	• *SoluteBindingProb* §	0.5	0.38	0.5	
	• *SoluteBindingCycles* §	11	28	10	
	MetabolizeProb §	0.02	0.02	0.02	METABOLISM Control
	SoluteScale[1] §	1.0	1.0	1.0	
Dosage Parameter and TIME	*a*	5,000	5,000	5,000	Dosage Parameters
	• *b* §	1	2	2	
	c	2	2	2	
	• *injectTime*	2.0	0.0	0.0	Bolus Injection TIME

[1] *SoluteScale* was called *ISL2WetLabScaling* by Park et al. (2009).

Figure 1

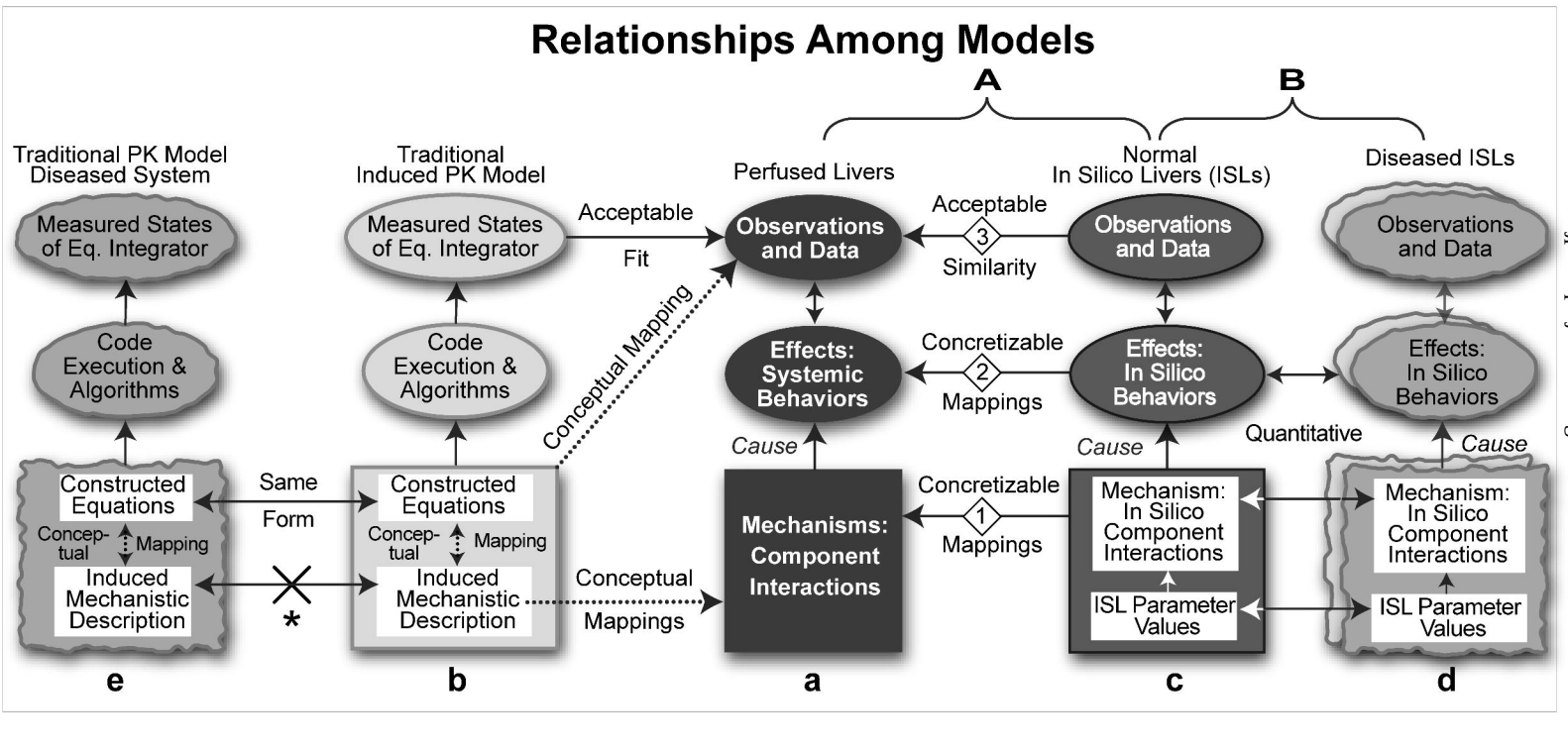

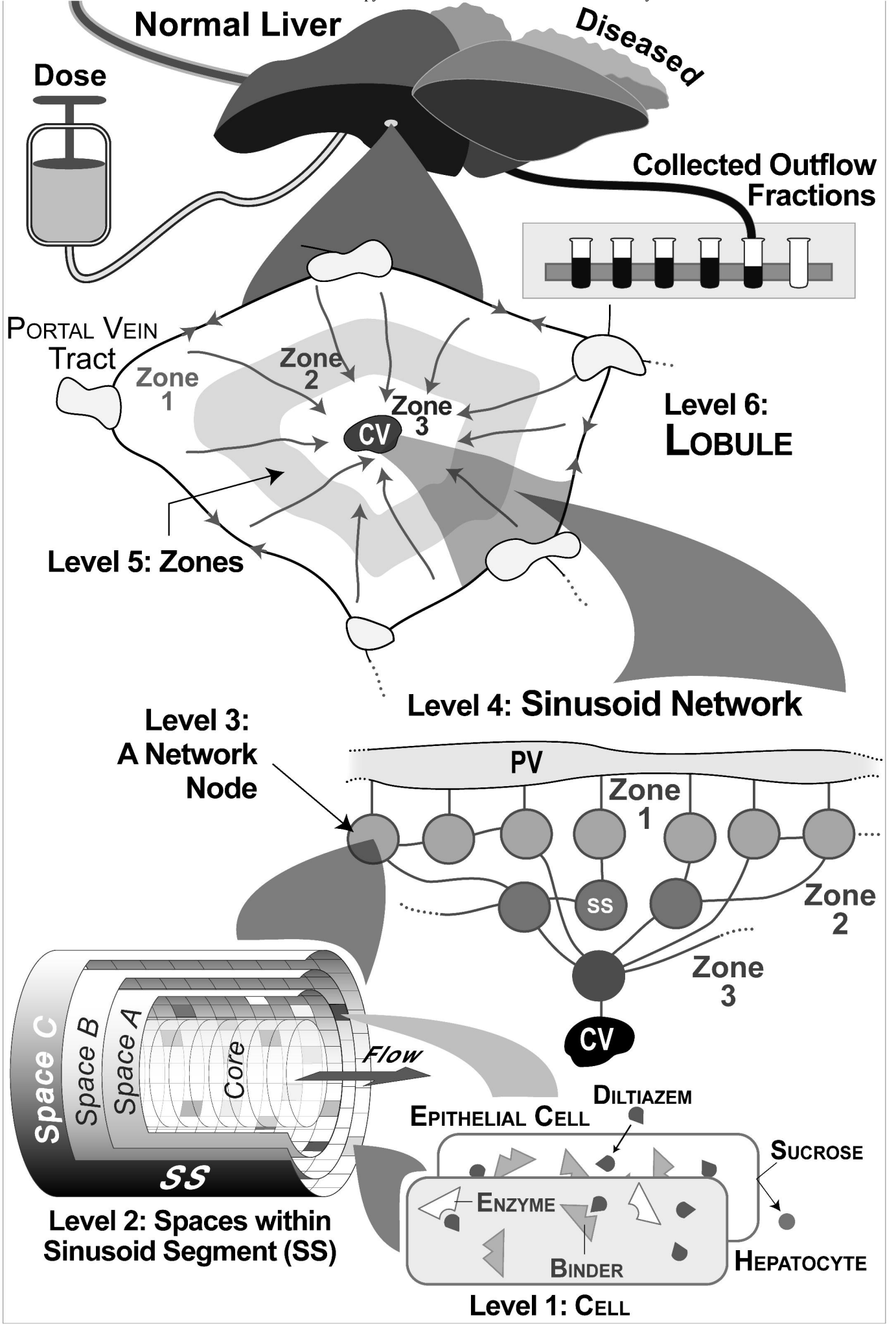
Normal Liver
Diseased
Dose
Collected Outflow Fractions
Portal Vein Tract
Zone 1
Zone 2
Zone 3
CV
Level 6: LOBULE
Level 5: Zones
Level 4: Sinusoid Network
Level 3: A Network Node
PV
Zone 1
SS
Zone 2
Zone 3
CV
Space C
Space B
Space A
Core
Flow
SS
Level 2: Spaces within Sinusoid Segment (SS)
Diltiazem
Epithelial Cell
Sucrose
Enzyme
Binder
Hepatocyte
Level 1: Cell

Figure 2

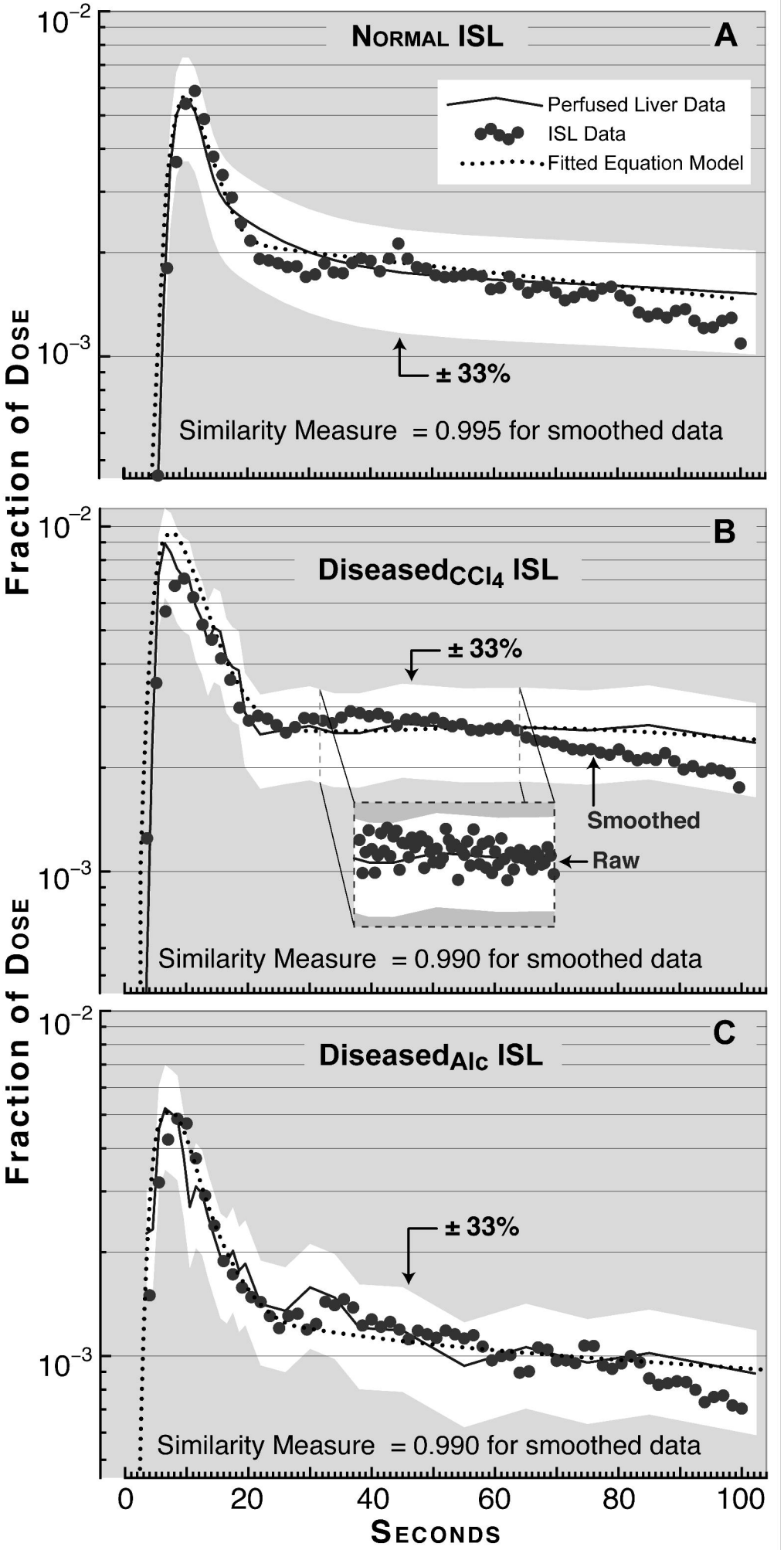
NORMAL ISL
A
Perfused Liver Data
ISL Data
Fitted Equation Model
± 33%
Similarity Measure = 0.995 for smoothed data
Fraction of Dose
10^{-2}
10^{-3}
B
Diseased$_{CCl_4}$ ISL
± 33%
Smoothed
Raw
Similarity Measure = 0.990 for smoothed data
C
Diseased$_{AIc}$ ISL
± 33%
Similarity Measure = 0.990 for smoothed data
0
20
40
60
80
100
SECONDS

Figure 3

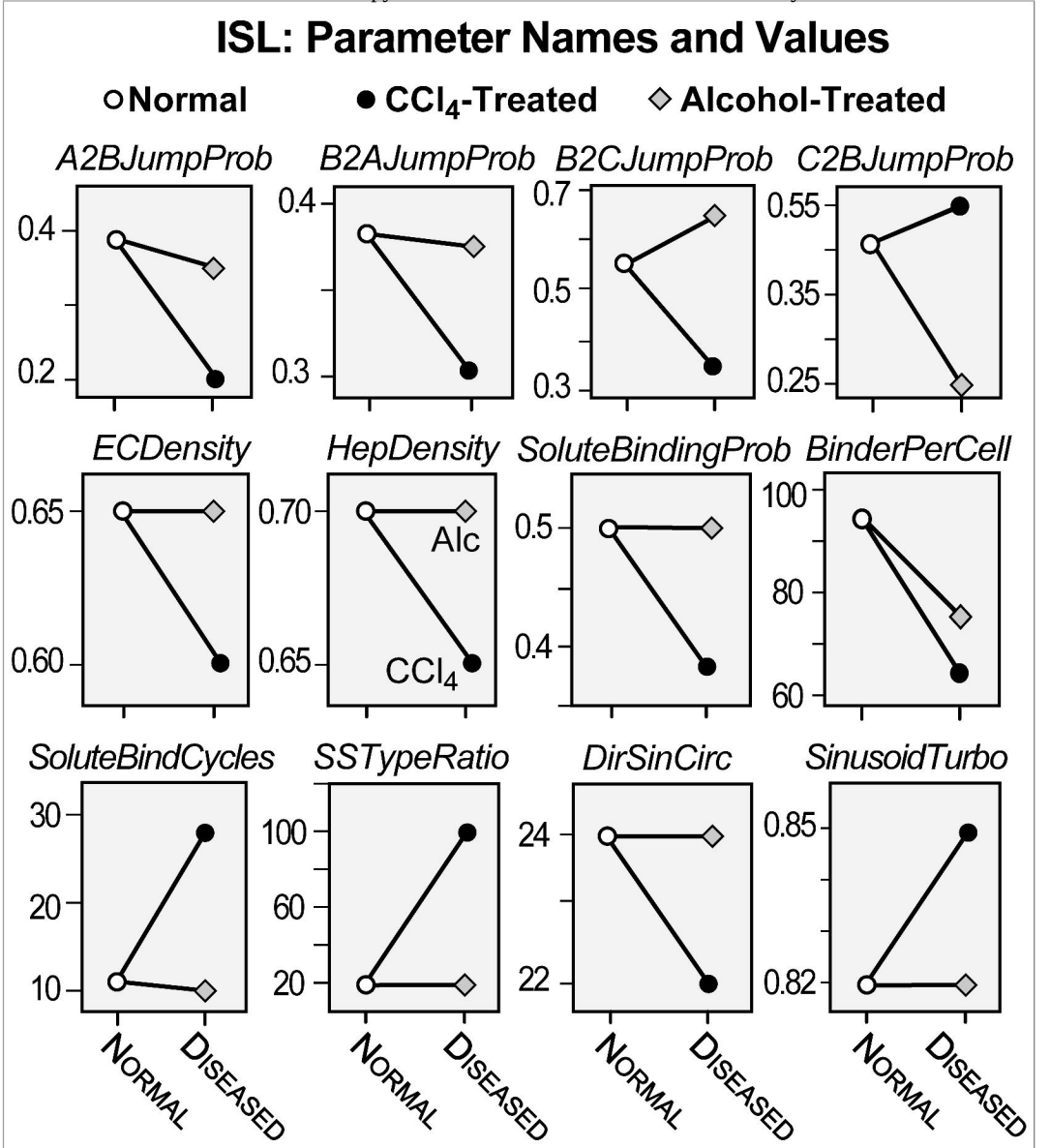
ISL: Parameter Names and Values
Normal
CCl4-Treated
Alcohol-Treated
A2BJumpProb
B2AJumpProb
B2CJumpProb
C2BJumpProb
ECDensity
HepDensity
SoluteBindingProb
BinderPerCell
Alc
CCl4
SoluteBindCycles
SSTypeRatio
DirSinCirc
SinusoidTurbo
NORMAL
DISEASED

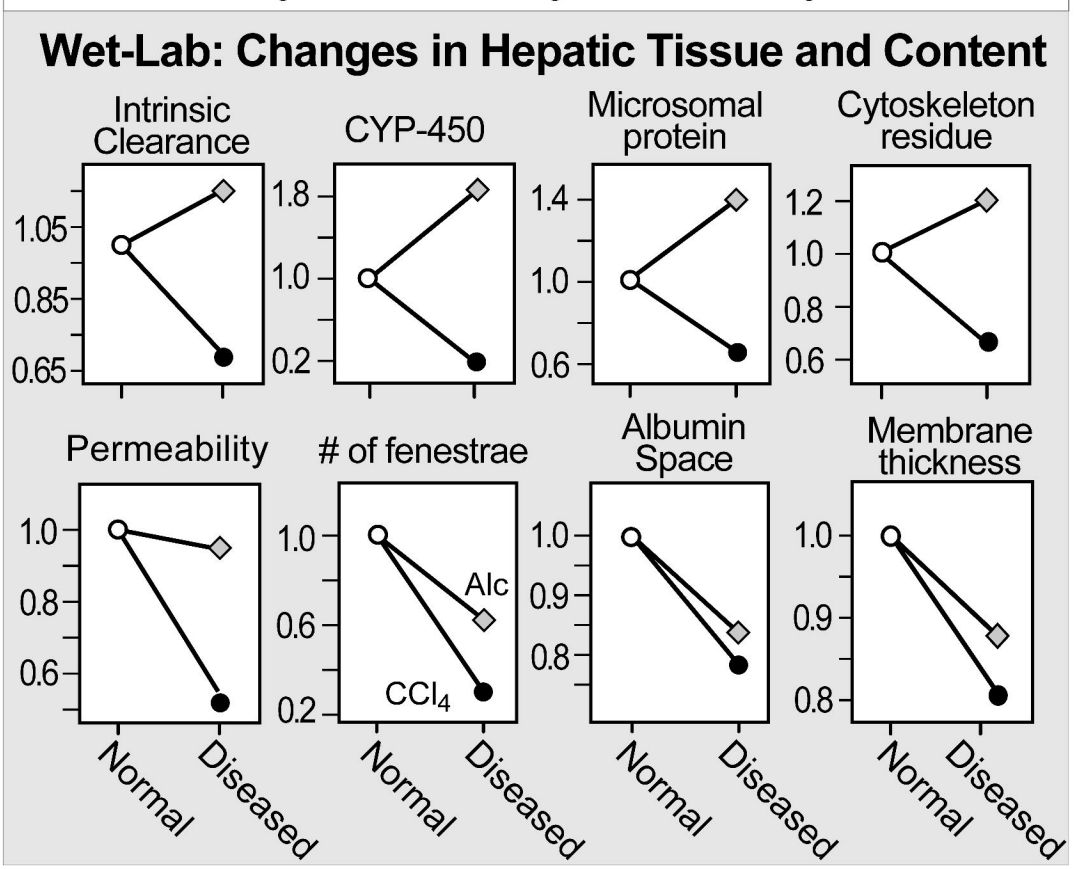
Wet-Lab: Changes in Hepatic Tissue and Content
Intrinsic Clearance
CYP-450
Microsomal protein
Cytoskeleton residue
Permeability
# of fenestrae
Albumin Space
Membrane thickness
Alc
CCl4
Normal
Diseased

Figure 4

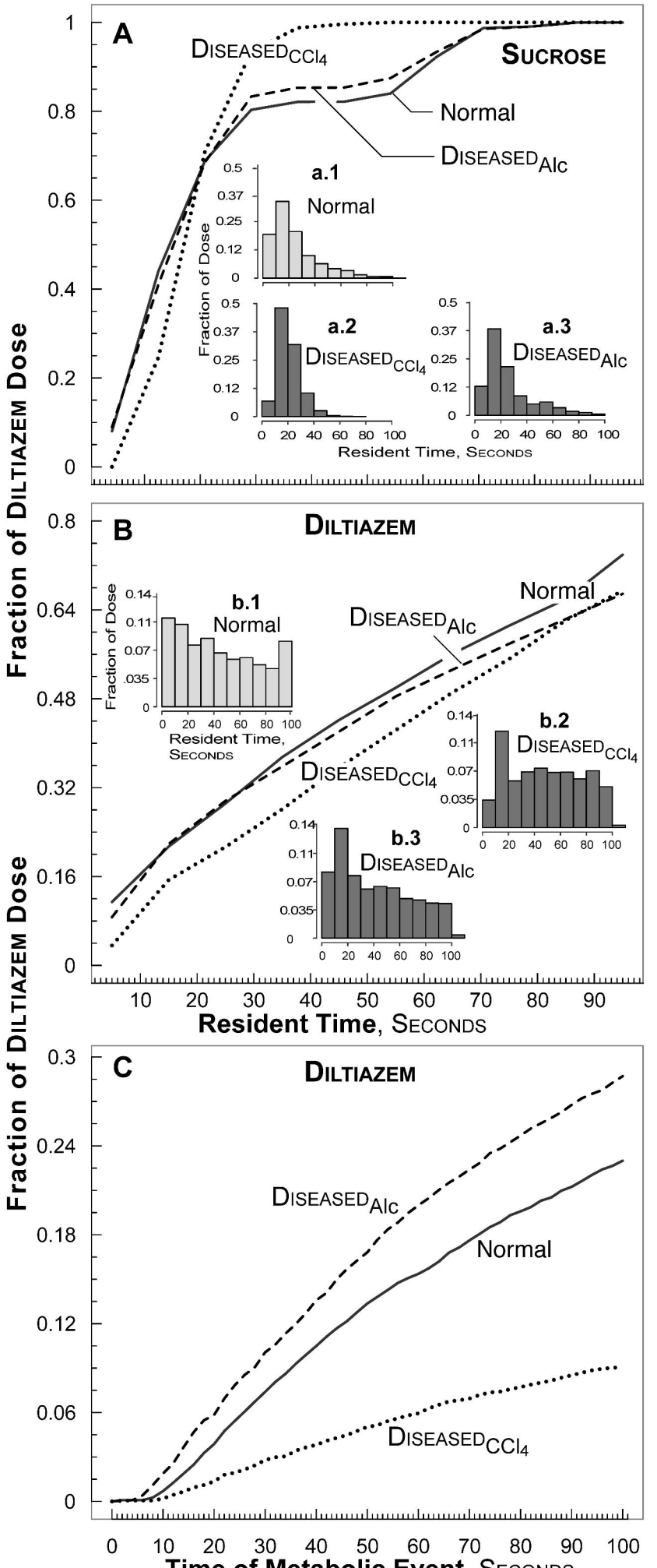
A
DISEASED$_{CCl_4}$
SUCROSE
Normal
DISEASED$_{Alc}$
a.1
Normal
a.2
DISEASED$_{CCl_4}$
a.3
DISEASED$_{Alc}$
Fraction of Dose
Resident Time, SECONDS
Fraction of DILTIAZEM Dose
B
DILTIAZEM
b.1
Normal
b.2
DISEASED$_{CCl_4}$
b.3
DISEASED$_{Alc}$
Resident Time, SECONDS
C
DILTIAZEM
Time of Metabolic Event, SECONDS

Figure 5

Figure 6

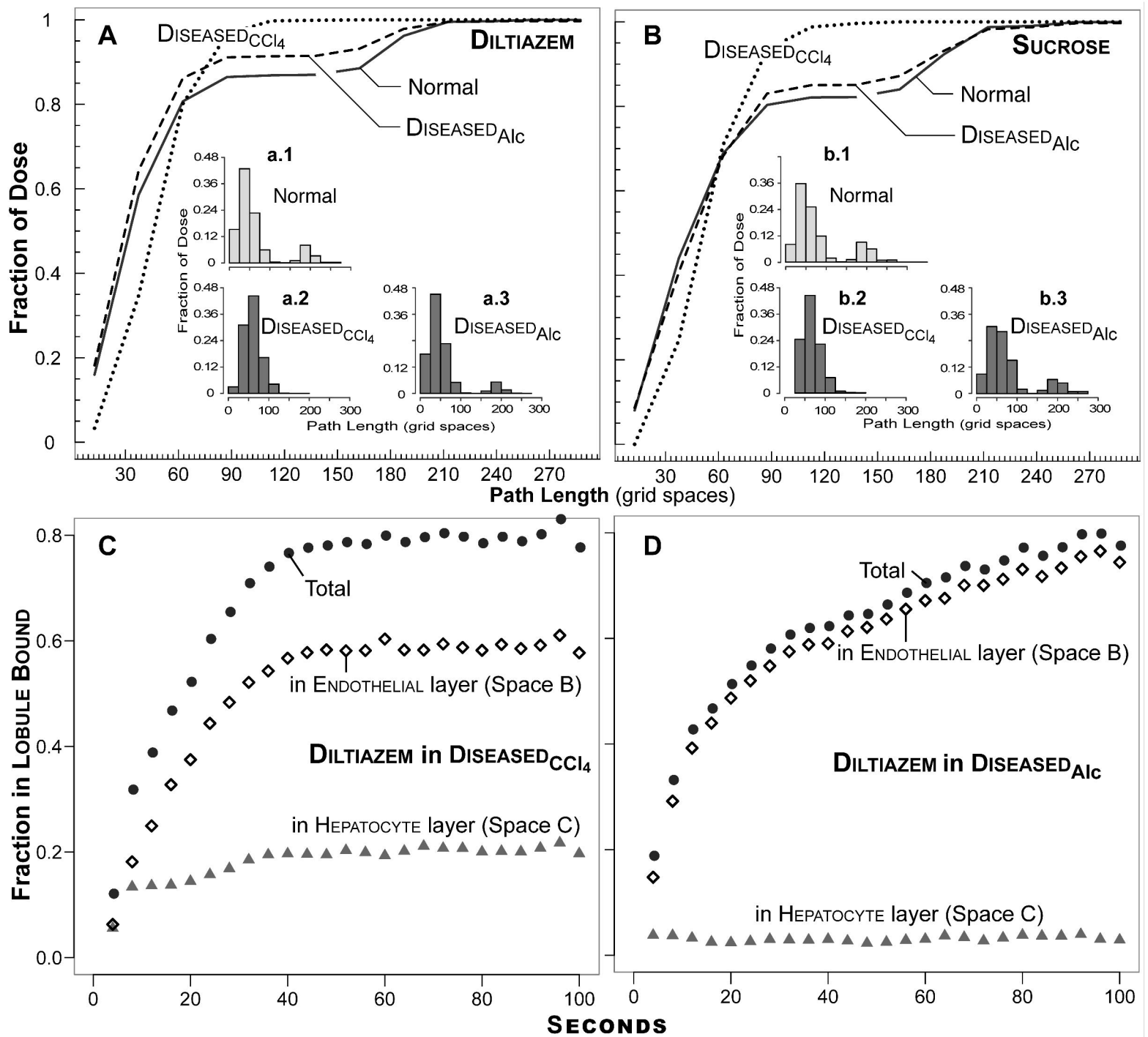
A
DISEASED$_{CCl_4}$
DILTIAZEM
Normal
DISEASED$_{Alc}$
a.1
Normal
a.2
DISEASED$_{CCl_4}$
a.3
DISEASED$_{Alc}$
Fraction of Dose
Path Length (grid spaces)
B
DISEASED$_{CCl_4}$
SUCROSE
Normal
DISEASED$_{Alc}$
b.1
Normal
b.2
DISEASED$_{CCl_4}$
b.3
DISEASED$_{Alc}$
Fraction of Dose
Path Length (grid spaces)
Path Length (grid spaces)

C
Total
in ENDOTHELIAL layer (Space B)
DILTIAZEM in DISEASED$_{CCl_4}$
in HEPATOCYTE layer (Space C)
D
Total
in ENDOTHELIAL layer (Space B)
DILTIAZEM in DISEASED$_{Alc}$
in HEPATOCYTE layer (Space C)
Fraction in LOBULE BOUND
SECONDS

Figure 7

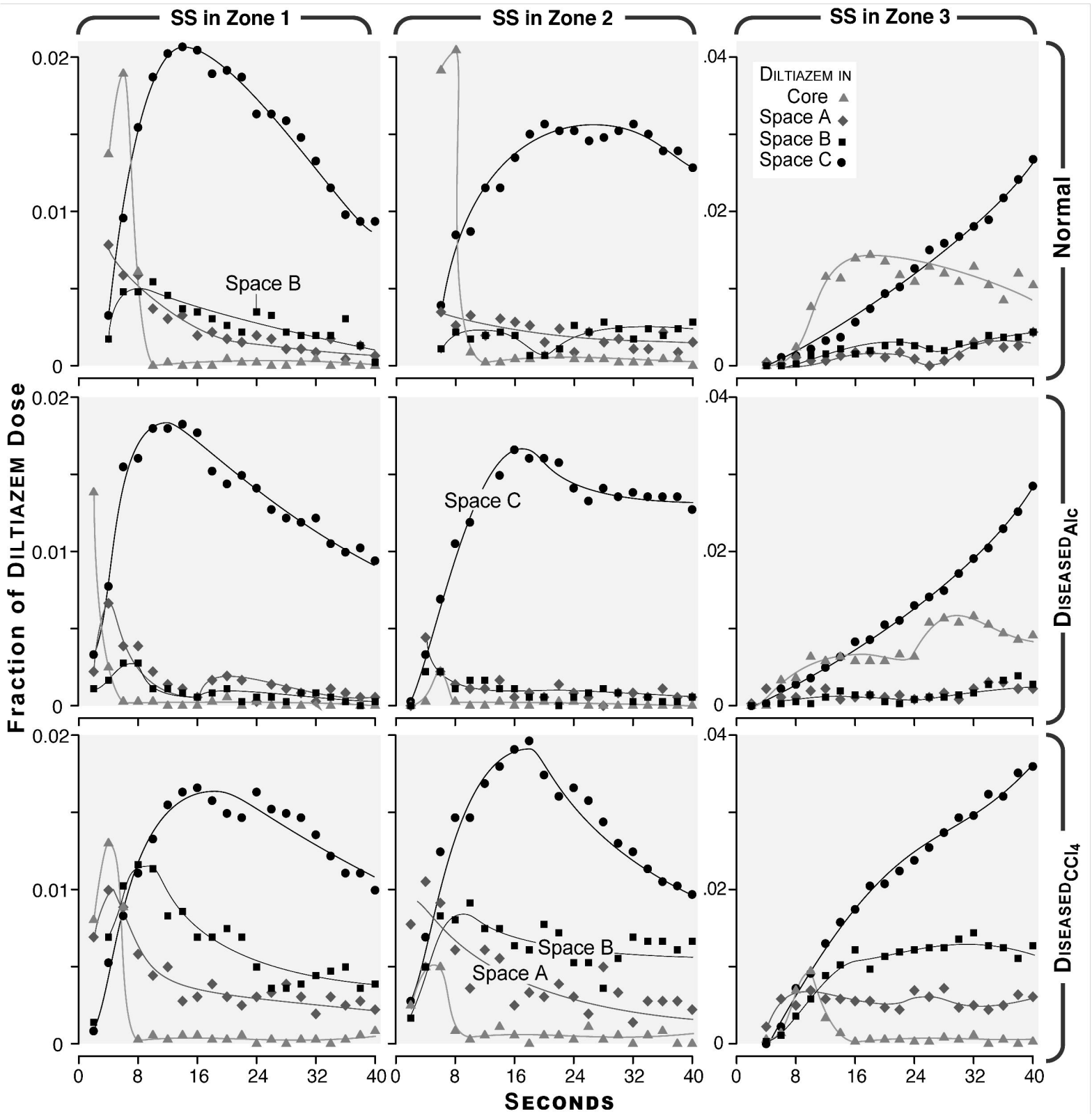
SS in Zone 1
SS in Zone 2
SS in Zone 3
Diltiazem in
Core
Space A
Space B
Space C
Space B
Space C
Space B
Space A
Normal
Diseased$_{AlC}$
Diseased$_{CCl_4}$
Fraction of Diltiazem Dose
Seconds
0.02
0.01
0
.04
.02
0
8
16
24
32
40

Figure 8

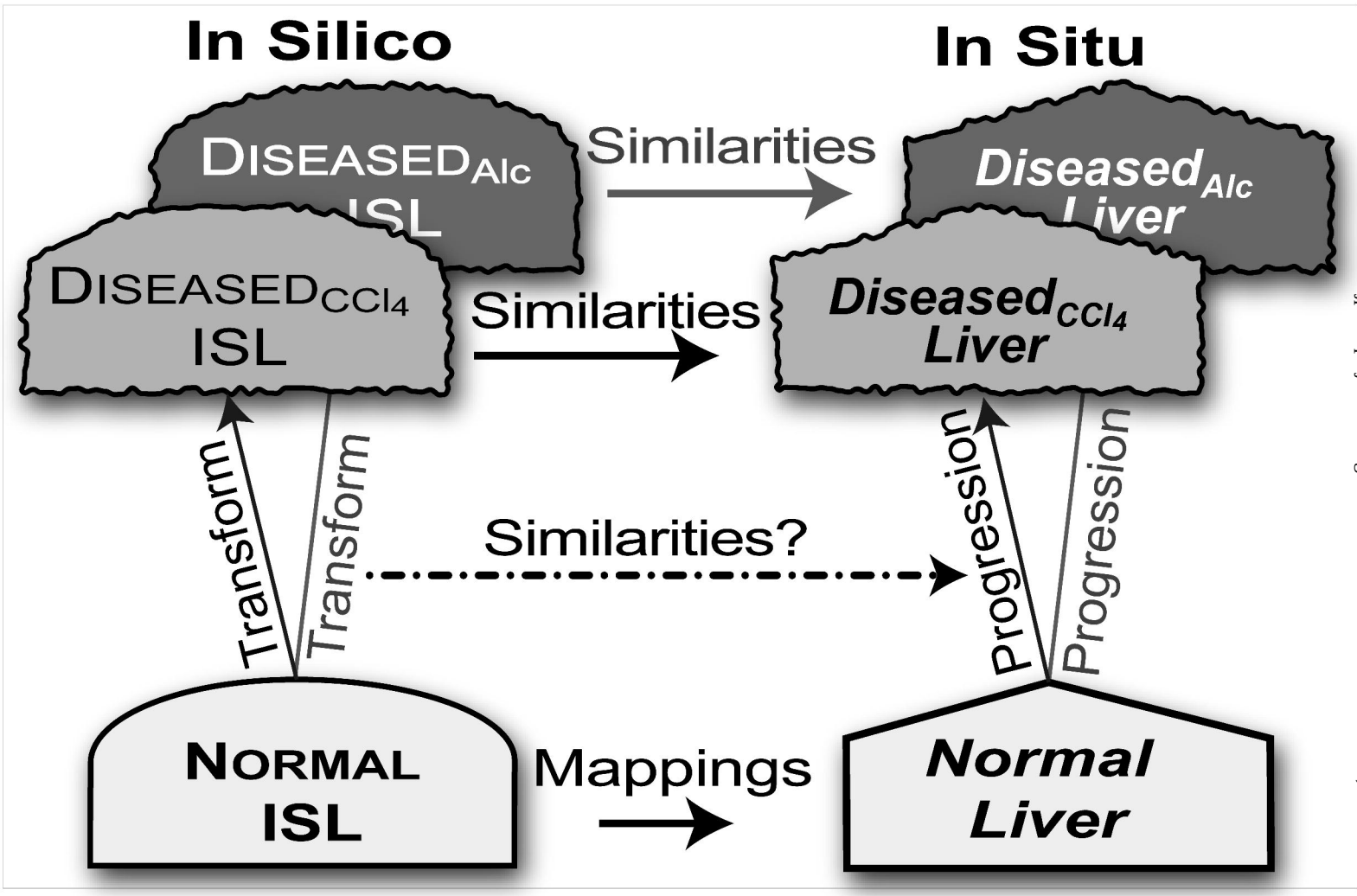

JPET Fast Forward. Published on April 20, 2010 as DOI: 10.1124/jpet.110.168526
This article has not been copyedited and formatted. The final version may differ from this version.

Appendix

Descriptions of key ISL parameters listed in Table 1

monteCarloRuns: The number of LOBULE simulations averaged to produce results for one ISL experiment

cycleLimit: Provides the simulation with a stopping criterion

StepsPerCycle: Specifies the number of iterations the *RefModel* executes in a single *ExperAgent* cycle. The *ExperAgent* cycle is grounded to the default time scale in the validation data.

nominalProfile: Specifies which model (e.g., *RefModel*) to use as the nominal when calculating SM values

GraphInputFile: Specifies the file to read if the SS graph is to be specified by an explicit graph (file format is GML)

GraphSpecFile: Provides the lobule graphical specification, and specifies the base file name (*extension.ls*) to be used if the graph is to be specified according to the LOBULE Specification file

GraphSpecIterates: Tells the framework to modify LOBULE specification and run a Monte-Carlo set (consisting of *N* runs) for each different LOBULE specification. Set to 1, it runs 1 set and provides 1 set of outputs. Set to 5, the first run uses the current contents of *lobule.ls*; it then runs 4 more sets, slightly modifying the LOBULE specification each time, resulting in 5 sets.

SSTypeRatio = DirSinRatio/*TortSinRatio*; *DirSinRatio* specifies the percentage of SS that are type $\boldsymbol{S}_A$ ("direct;" shorter and wider); *TortSinRatio* specifies the percentage of SS that are $\boldsymbol{S}_B$ ("tortuous;" longer and thinner)

DirSinCirc: circumference for each $\boldsymbol{S}_A$ type SS. Although fixed for this study, $\boldsymbol{S}_A$ SS circumference can be randomly drawn from a uniform distribution having the range *DirSinCircMin* and *DirSinCircMax*.

TortSinCirc: circumference for each $\boldsymbol{S}_B$ type SS. Although fixed for this study, $\boldsymbol{S}_B$ SS circumference can be randomly drawn from a uniform distribution having the range *TortSinCircMin* and *TortSinCircMax*.

DirSinLenAlpha, DirSinLenBeta, DirSinLenShift: These values set the parameters for a pseudo-random number generator using a modified form of the Gamma distribution; the modification consists of a left-right shift of the distribution, allowing the user to clip off the front of the distribution. The pseudo-random number drawn is the length of a specific shorter, wider SS.

TortSinLenAlpha, TortSinLenBeta, TortSinLenShift: These values set the parameters for a pseudo-random number generator using a modified form of the Gamma distribution; the modification consists of a left-

JPET Fast Forward. Published on April 20, 2010 as DOI: 10.1124/jpet.110.168526
This article has not been copyedited and formatted. The final version may differ from this version.

right shift of the distribution, allowing the user to clip off the front of the distribution. The pseudo-random number drawn is the length of a specific longer, thinner SS.

A2BJumpProb: Specifies the probability that, when given the option, a COMPOUND will jump from Space A to Space B

B2AJumpProb: Specifies the probability that, when given the option, COMPOUND will jump from Space B to Space A

B2CJumpProb: Specifies the probability that, when given the option, COMPOUND will jump from Space B to Space C

C2BJumpProb: Specifies the probability that, when given the option, COMPOUND will jump from Space C to Space B

CoreFlowRate: The number of slots (grid spaces) COMPOUNDS in the SS Core move forward during each step

SinusoidTurbo: The PV to CV bias applied to the otherwise random walk for COMPOUNDS in grid spaces of an SS. Smaller turbo means greater tendency of any one COMPOUND to wander sideways or backwards. Larger Turbo means a stronger flow from the input to the output of the SS

ECDensity: Specifies the relative ENDOTHELIAL CELL density; given the grid dimensions of Space B of a given SS, it specifies the percentage of spaces that index an ENDOTHELIAL CELL

HepDensity: Specifies the relative HEPATOCYTE density; given the grid dimensions of Space C of a given SS, it specifies the percentage of spaces that index a HEPATOCYTE

BindersPerCel: in this study, the number of BINDERS inside each CELL. They are simple BINDERS for ENDOTHELIAL CELLS and ENZYMES for HEPATOCYTES. The ISL provides the option to randomly draw the number of BINDERS for each CELL from a uniform distribution having limits of *BindersPerCellMin* and *BindersPerCellMax*

MetabolizeProb: Probability that an ENZYME will transform DILTIAZEM to a METABOLITE before it releases it

SoluteBindingProb: Probability that, when a BINDER and COMPOUND make contact, the COMPOUND will be bound

SoluteBindingCycles: Number of simulation cycles a binder holds a COMPOUND. This value maps to observing that the fraction bound within the same small region of a lobule is unchanged over an interval

JPET Fast Forward. Published on April 20, 2010 as DOI: 10.1124/jpet.110.168526
This article has not been copyedited and formatted. The final version may differ from this version.

isMembraneCrossing: Specifies whether the COMPOUND can cross into (and out of) a CELL or not; DILTIAZEM can; SUCROSE cannot

SoluteScale: (called *ISL2WetLabScaling* by Yan et al. (2008a,b)) Provides the precise validation mapping from ISL output to the wet-lab output fraction for that compound

• Supplementary Material •

Tracing Multi-Scale Mechanisms of Drug Disposition in Normal and Diseased Livers

Sunwoo Park, Sean H.J. Kim, Glen E.P. Ropella, Michael S. Roberts,
and C. Anthony Hunt

Validation and comparison of outflow profiles. ISL outflow profiles for four simulated cationic drugs in identically parameterized NORMAL ISLs were validated earlier against in situ referent profiles (Yan et al., 2008a,b,c). Disposition of DILTIAZEMS in the same NOMRAL ISLs and in a related, $\text{DISEASED}_{\text{CCl4}}$ ISLs were similarly validated using the same SM . The referent livers for the $\text{DISEASED}_{\text{CCl4}}$ ISLs came from rats chronically treated with CCl_4. The original citation (hung et al., 2002b) contains histopathology details. For this report, the diltiazem outflow profiles from those same CCl_4–treated livers were again matched by DILTIAZEM outflow profiles, but from a somewhat different, $\text{DISEASED}_{\text{CCl4}}$ ISL: the match provided by the $\text{DISEASED}_{\text{CCl4}}$ ISLs in this report were improved over that reported earlier in (Park et al., 2009) by adjusting eleven rather than nine key parameters. In addition, diltiazem outflow profiles from alcohol–treated livers were matched by DILTIAZEM outflow profiles from new, $\text{DISEASED}_{\text{ALC}}$ ISLs. The referent livers of the $\text{DISEASED}_{\text{ALC}}$ ISLs came from rats chronically treated with ethanol (Hung et al., 2002a). For both sets of experiments, SUCROSE was used as an EXTRACELLULAR marker. Outflow profiles from $\text{DISEASED}_{\text{CCl4}}$ ISLs and $\text{DISEASED}_{\text{ALC}}$ ISLs were accepted initially as valid when SM > 0.8. The iterative refinement protocol described in (Park et al., 2009) was used to further improve the parameterization so that SM > 0.9 were achieved.

Similarity Measure. An ISL outflow profile was accepted as valid—as being indistinguishable experimentally from a profile obtained from a repeat wet-lab experiment—when SM > 0.8. Once that was achieved, it was increased to SM > 0.9. ISL outflow profiles were compared with referent profiles using the quantitative SM used previously (Hunt et al., 2006; Yan et al., 2008a,b; Park et al., 2009). It is the fraction of collected COMPOUNDS that lies within a band that was a prespecified, scaled factor of referent outflow values. We used

$$SM_1(p_s, p_r, s, e, k) = \frac{\sum_{i=s}^{e} \mathcal{C}(p_r^l(i,k) \le p_s(i) \le p_r^u(i,k))}{(e - s + 1)}$$

where p_s: simulated hepatic disposition outflow profile; p_r: in situ hepatic disposition outflow profile; $s,e \in \mathbf{Z}^+$: start and end simulation cycle number; m: sample mean of p_r; $\gamma_r = (p_r - \mu)/\mu$; $k \in R^+$: scaling factor of the $\pm k \cdot \sigma(\gamma_r)$ band; $p_r^l(i,k) = p_r(i)(1 - k \cdot \sigma(\gamma_r))$: lower bound of the band; $p_r^u(i,k) = p_r(i)(1 + k \cdot \sigma(\gamma_r))$: upper bound of the band; $\sigma(\gamma_r)$: standard deviation of γ_r; $C(cond) = 1$ if the *cond* is true, otherwise, 0; a counting function $\{F,T\} \rightarrow \{0,1\}$; and $\boldsymbol{Z}$ is a set of integer values, $\boldsymbol{R}$ is of the real numbers $(0, \infty^+)$; $k = 0.5$, 0.75, and 1.0 were used. Both raw and smoothed ISL profiles were scored.

Drug input and dosage time management. ISL experiments followed the same dosing protocol used in situ (Yan et al., 2008a,b; Park et al., 2009). As illustrated in Fig. 2, a bolus dose of SCUROSE and/or DILTIAZEM was injected into a simulated catheter that feeds into PV. COMPOUNDS were collected as they entered CV, simulating collection by a fraction collector.

Hung et al. used the sum of two inverse Gaussian density functions (requiring five-parameters) to simulate compound dilution and dispersion within catheters and perfusion tubing before and after the lobular level (Hung et al., 2002a). They fitted the density functions to averaged outflow profiles obtained following their standard experimental protocol when the liver was replaced by a shunt. They used that dosing function to correct outflow profiles prior to PK analysis. We obtained identically shaped dosing curves using the three-parameter density function, *d(t)*; we parameterized *d(t)* to provide quantitative control of COMPOUND input into PV and to simulate all influences on diltiazem in situ prior to reaching PV and after exiting CV. Park et al. (2009) proved an example of a parameterized *d(t)* in their Fig. 2.

$$d(t) = a * \frac{b^c * t^{c-1} * e^{-b*t}}{(c-1)!}$$

a, b, and c determine the dose input function's amplitude, location, and shape; t is time and e is an exponential function. The injection model $D(a,b,c)$ uses $d(t)$. Different values of a, b, and c can be used when catheter, perfusion and/or collection details change, and when different pathological liver states alter the path from injection to PV or following CV (Park et al., 2009). Different dosage injection models *D*(*5000,1,2*) and *D*(*5000,2,2*) were used for the validation of NOMRAL and both DISEASED ISLs, respectively. Different injection models were needed because diltiazem was detected earlier in the collected outflow perfusate from both types of diseased relative to normal livers.

ISL profiles were also compared to that of the existing mathematical models – two-phased stochastic liver model (TPSLM). We used Hollenbeck's (1998) implementation of de Hoog's (1982) numerical inverse Laplace transform algorithm to compute numerical inverse Laplace transforms of the TPSLM) (Hung et al., 2001, 2002a)[3, 15]. TPSLM predicts hepatic disposition of an in situ rat liver using Laplace transform and its inverse form. It uses the following equation to predict hepatic disposition of COMPOUNDS.

$$C_{drug}(t) = \frac{Dose}{Q} L^{-1}\{\hat{f}_{cath}(s)\hat{f}_{y,w}(s)\}$$

Dose is the injected drug bolus and Q is the perfusion rate. $L^{-1}[\cdot]$ denotes the inverse Laplace transform.

$\hat{f}_{cath}(s)$ is the Laplace transform of the transit time density function of U-^{14}C sucrose molecules across the liver.

$$\hat{f}_{cath}(s) = \hat{f}_B(s + k_{in}(1 - \hat{f}_y(s)))$$

k_{in} is the influx rate constant from a sinusoid into to hepatocytes.

$\hat{f}_B(s)$ is the Laplace transform of the transit time density function of the nonpermeating indicator.

$$\hat{f}_B(s) = p\hat{f}_1(s) + (1-p)\hat{f}_2(s)$$

$\hat{f}_1$ and $\hat{f}_2$ are Laplace transforms of the inverse Gaussian density function with MT_1 and CV_1^2, and MT_2 and CV_2^2, respectively. MT_1 and CV_1^2 are mean and standard deviation of $\hat{f}_1(t)$. MT_2 and CV_2^2 are mean and standard deviation of $\hat{f}_2(t)$.

$$\hat{f}_{y,W}(s) = \frac{k_{in,w}/v_{c,w}}{k_{in,w}/v_{c,w} + s}$$

$\hat{f}_{y,w}(s)$ is the Laplace transform of the transit time density function of water $\hat{f}_W(s)$.

$k_{in,w}$ is permeation constant. $v_{c,w}$ is the normalized water volume, V_B/V_C.

$$\hat{f}_1(s) = exp\left(\frac{1}{CV_1^2} - \left(\frac{MT_1}{CV_1^2/2}\left(s + \frac{1}{2MT_1CV_1^2}\right)\right)^{1/2}\right)$$

$$\hat{f}_2(s) = exp\left(\frac{1}{CV_2^2} - \left(\frac{MT_2}{CV_2^2/2}\left(s + \frac{1}{2MT_2CV_2^2}\right)\right)^{1/2}\right)$$

Table 1. *RefModel* is a two-phase stochastic PK liver model. Listed are the parameters and values used to fit the referent PK data.

Category	Parameter	Normal	Diseased_{CCl4}	Diseased_{ALC}
Fixed Parameters	Q	2[a]	2[a]	2[a]
	$Dose$	15[a]	15[a]	15[a]
	k_{on}	0.35[b]	0.35[b]	0.35[b]
	k_{off}	0.021[b]	0.021[b]	0.021[b]
	K_S	16.67	10.59	23.56
	K_R	0.95	0.95	0.95
	CL_{int}	67.41[c]	45.99[c]	77.25[c]
	CL_{pt}	25.35[c]	25.35[c]	25.35[c]
	PS	90.54[c]	46.44[c]	83.76[c]
	V_B	0.49[d]	0.57[d]	0.53[d]
	V_C	1.30[d]	1.34[d]	1.38[d]
Derived Parameters	$k_{out,w}$	$k_{out,w}$	$v_{c,w}\ k_{in,w}$	$v_{c,w}\ k_{in,w}$
	$k_{ior,w}$	$k_{ior,w}$	$k_{in,w} / k_{out,w}$	$k_{in,w} / k_{out,w}$
	k_e	CL_{int} / V_C	CL_{int} / V_C	CL_{int} / V_C
Estimated Parameters	$v_{c,w}$	5 (V_C / V_B)	5 (V_C / V_B)	5 (V_C / V_B)
	$k_{in,w}$	0.00815(CL_{pt} / V_B)	0.01250(CL_{pt} / V_B)	0.00695(CL_{pt} / V_B)
	MT_1	11.975	10.075	9.875
	MT_2	67.575	108.575	65.575
	CV_1^2	0.282	0.252	0.252
	CV_2^2	0.671	0.571	0.771
	p	0.675	0.645	0.645
Units:	[a] $ml \cdot min^{-1}$	[b] sec^{-1}	[c] $ml \cdot min^{-1} \cdot g^{-1}$	[d] $ml \cdot g^{-1}$

In Silico Liver Grounding. In order to develop and begin validating concretized theories about the progression from normal to disease states and how hepatic features interact with compounds, we need the ability to simultaneously explore different regions of plausible mechanism space at different levels of detail, and relate results to wet-lab observations. To facilitate that process it must be easy to change mechanistic details at any level without having to invest significant time in ISL reengineering. We have discovered that the best way to achieve those objectives is to remove metric grounding from ISLs. Hunt et al. (2009) discuss the merits of doing so.

The units, dimensions, and/or objects to which a variable or model constituent refers establish groundings. Inductive ordinary differential equation models are typically grounded to metric spaces. So doing provides simple, interpretive mappings between output and parameter values and referent data. Because phenomena and generators are tightly coupled in such models, the distinction between phenomenon and generator is often small. However, metric grounding creates issues that must be addressed each time one needs to expand the model to include additional phenomena and when combining models to form a larger system. Adding a term to an equation, for example, requires defining its variables *and premises* to be quantitatively commensurate with everything else in the model. Such expansions can be challenging and even infeasible when knowledge is limited and uncertainty is high, which is the situation that we faced. A model synthesized from components all grounded to the same metric spaces is itself grounded to the Cartesian composite of all those metric spaces. The solution is to remove metric grounding from the ISL and confine it to quantitative feature-to-feature and phenomena-to-phenomena mapping models.

The micromechanisms responsible for generation of hepatic disposition data during a perfused liver experiment do not interact according to any external measurement methods. Nor do they interact directly with the whole rat. They interact with the other components around them. Hepatic cells, for example, interact with each other and their local environment. They are independent of any measures used by an outside observer. From that fact, we inferred that the ISLs must employ similar internal organization, which in modeling terms, means each component is grounded to other components rather than to a metric imposed by an outside observer: they are relationally grounded.

On Differences Between Traditional PK Models and Synthetic Analogues. The above observations motivate comment about the differences between traditional, inductive, equation based PK models (left side of Fig. 1) and synthetic, internally grounded analogues like ISLs. In models grounded to metric spaces, parameters serve mostly to shift model behavior within a smooth region of the output metric space. In models grounded to hyperspaces or in those that are relationally grounded, like ISLs, parameters serve that same function. They also serve to discontinuously (even abruptly) shift the behavior of the model into an entirely different region of behavior space: they change the analogue's dynamic phenotype. In metrically grounded models, the character of the model is bounded, whereas in relational or hyperspace grounded models, model character can change completely with a change in parameters. In the former case, parameters describe one, particular (though abstract) model type. In the latter case, parameters describe families of different yet related models. The DISEASED ISLs are examples. Relational grounding enables flexible, adaptable analogues, but requires a separate analogue-to-referent mapping model.

Tracing and Computation Granularities. When the granularity of the tracing is not the same as the very finest grain of the computation, then events below that tracing granularity are invisible. An example is that during a single simulation cycle, it is possible for a COMPOUND to take a path of (1) $SS_A \rightarrow SS_B \rightarrow SS_C$ or (2) $SS_A \rightarrow SS_D \rightarrow SS_A$. In the first case, the COMPOUND traverses two SS nodes in a single cycle. This prevents a complete trace. We cannot detect that the COMPOUND visited SS_B. In the second case, the COMPOUND traverses back to its starting location, so potentially we might not get any tracing results for that COMPOUND. Additionally, if a large number of steps (e.g., 10 or 20 steps) had been executed per simulation cycle, we might, in theory, not get any tracing results for some COMPOUNDS because they would have reached the CV or been metabolized within a single simulation cycle. The current ISL solves the above problems by conducting profile validation in the cycle level (coarse-grain) and tracing in the step level (fine-grain). Although the simulation uses a logical concurrency model, which allows us to

consider steps as a number of parallel events in a single cycle, those events are serialized (by interleaving) within the cycle and we can index the trace by position in the sequence.

In such situations, it is tempting to ground the model absolutely to, say, time in seconds. Note that for purposes of describing the traces, we do that. The interval between two adjacent cycles is divided by the number of steps. The quotient of the division is a new fine-grain time resolution for tracing. In the current ISL, time resolution in the cycle level is 0.5 SECONDS and the number of steps per cycle is 2. For these traces, time resolution in the step level then becomes 0.25 SECONDS (0.5/2). But, methodologically, it is important to note that this is a post-simulation analytic technique for which there is no referent counterpart.

ISL Implementation and Execution. Parallel executions were performed in different ways to improve performance compared to monotonic parallelism and sequential execution (Ropella et al., 2003). Each parallel mode was associated with one of the six ISL levels illustrated in manuscript Fig. 3 or an experimental requirement. Heterogeneity in parallel execution helped achieve improved performance along with efficient resource management. ISL parallel mode, illustrated in Fig. S1, was supported at group and experiment levels. Group Level Parallel mode enabled executing multiple experiments in parallel by segregating each and allowing each to run concurrently without interaction. Parallel batch processing and analysis of local execution results were performed using that mode. Experiment Level Parallel mode enabled executing single experiments in parallel as separate LOBULE Monte Carlo variants.

Tools used. We built the environment using Swarm 2.2 (www.swarm.org), MPICH (www-unix.mcs.anl.gov/mpi/mpich1/) 1.2, GCC (gcc.gnu.org) 4.1.1, OSCAR (oscar.openclustergroup.org) 5.0, and Fedora 5 (www.fedoraproject.org) on a small-scale, in-house, eight-node Beowulf cluster. Simulation and tracing results were analyzed using R (www.r-project.org) 2.7.1 and Matlab (www.mathworks.com) 7.14.

Generating Raw Event Trace Data. During the first phase, two types of raw tracing data were generated for SSs and METABOLITES. A trace data file was generated for each SS including PV and CV. It recorded the temporal order of spatiotemporal events experienced by all COMPOUNDS that resided within a particular SS. The collected trace data were grouped into three fields – *simulation time*, *node*, and *compound*. The *simulation time* field provided an execution step counter value and simulation TIME, using the fine-grain time resolution (0.25 SECONDS) for each traceable event. The *graph node* field provided SS identifier (ID), SS length in grid spaces, and number of COMPOUNDS. It was used mainly to compute a COMPOUND'S traverse path length. The number of COMPOUNDS provided the population density of COMPOUNDS within a SS during a simulation cycle. The *compound* field provided spatiotemporal activities of COMPOUNDS within a SS. It grouped information into *compound ID*, *compound type*, *layer*, *spatial location*, *bound/unbound*, and *number of compounds*. *Compound ID* denoted the unique identifier of each COMPOUND, either DILTIAZEM or SUCROSE. *Layer* designated the COMPOUND'S "vertical" location within a SS: within Core or Spaces A, B, or C. *Spatial location* stated the COMPOUND'S coordinates within a space. The *bound/unbound* field recorded which component had bound a DILTIAZEM. It was set to *-Binder-*, *-Enzyme-*, *+ECell+*, *+Hepatocyte+*, or *NA* to indicate a DILTIAZEM'S location within the SSs in addition to its binding status. The *-Binder-* and *-Enzyme-* labels identified the compound as being bound to a BINDER in an ENDOTHELIAL CELL or to an ENZYME in a HEPATOCYTE; when unbound, the COMPOUND was labeled *+ECell+* or *+Hepatocyte+*. B*ound/unbound* was declared *NA* when the DILTIAZEM was located outside CELLS within any space. To trace METABOLIC events, each SS NODE also generated a tracing file that listed the COMPOUND'S ID and type along with the TIME METABOLISM occurred.

Additional Observations On Results

Validation of Disposition in NORMAL and DISEASED ISLs. The following is an illustration of iteratively adjusting parameters of the validated NORMAL ISL toward those of DISEASED$_{ALC}$ ISLs. PERFUSATE flow through each SS and the extent of local movement bias were controlled by two parameters: *CoreFlowRate* and *SinusoidTurbo*. For simplicity, the value of the former was held constant for all LIVERS. *SinusoidTurbo* controls COMPOUND movement within EXTRAVASCULAR, EXTRACELLULAR spaces. Changes in compound properties and/or changes in extravascular space properties can influence compound movement within extravascular, extracellular spaces, so *SinusoidTurbo* was available to change if needed (which it was). We first needed to adjust the probabilistic movements of COMPOUNDS in DISEASED$_{ALC}$ so that the outflow fraction near the peak (< 15 SECONDS) was close to that of a NORMAL outflow profile, but lower after 15 SECONDS. To achieve the first, we tuned *A2BJumpProb* and *B2AJumpProb* to values smaller than those of the validated NORMAL ISLs. When using the same dosing function, the shape and height of an outflow profile around its peak were very sensitive to changes in those two parameters. We also tuned *BinderPerCell* for DISEASED$_{ALC}$ to be smaller than those of NORMAL ISLs. That adjustment also contributed to the placement of the outflow profile's peak because it determined the population densities of BINDERS and ENZYMES in Spaces B and C. To achieve a lower outflow fraction after the peak, we increased *B2CJumpProb* but lowered *C2BJumpProb* relative to the values of NORMAL ISL. Consequently, more COMPOUNDS entered Space C in DISEASED$_{ALC}$, but they were delayed in reaching CV. An increase in METABOLIC events in Space C was also an important factor contributing to a lowered outflow profile. Other adjustments that enabled achieving SM > 0.9 are diagrammed in manuscript Fig. 4 and listed in Table 1.

Hunt et al. (2006) discuss analyses of ISL parameter changes and their sensitivity along with the fact that the generative consequences of all ISL parameters are networked. Adjusting other parameters can often offset a change in an outflow profile caused by a small change in one parameter. Consequently, studies of sensitivity to individual parameters are less informative and less meaningful than are location changes in LOBULE parameter space. Individually, the parameter changes in manuscript Fig. 4 did not cause statistically distinguishable changes in outflow profiles. Nevertheless, someone experienced in observing different ISL outflow profiles may observe a perceptible change in outflow profile shape. In general, a 5% change in any one parameter will produce an imperceptible change in an outflow profile and no change in SM value. However, a 5% change in all parameters can cause a significant change in outflow profile. The changes in manuscript Fig. 4 averaged 31.9% for DISEASED$_{CCl4}$ ISLs and 18.1% for DISEASED$_{ALC}$ ISLs.

Tracing COMPOUND Resident TIMES and METABOLIC Events. One COMPOUND within one SS grid space in manuscript Fig. 3 can be viewed as mapping to a wet-lab lower limit of detection. For example, it may be viewed as the limit of detection of referent compound in a biopsy sample that has a volume 1/5,000th that of an average lobule. At that limit, some biopsy samples will test negative for compound, even though we are confident some is present. By analogy, an empty space within the ISL during simulation cycle maps to "no detectable drug." Even though we can trace the change in location of a specific COMPOUND during execution, there is no mapping to corresponding changes in location for specific molecules. A COMPOUND maps to some number of actual molecules. From one simulation cycle to the next, that number of molecules is unchanged. However, the actual molecules to which a COMPOUND maps is not the same from one simulation cycle to another.

From raw COMPOUND tracing data, any number of derived measures can be obtained, and each enables viewing disposition from different perspectives. Each provides a somewhat different image of events occurring within ISLs during simulations. Some measures may be

useful in helping us think about ISLs (e.g., what change may be needed during parameter tuning to move closer to targeted phenomena). Others may be helpful in thinking about hepatic disposition. Still others may be helpful in thinking about different disease consequences and even disease progression.

Tracing COMPOUND Path Lengths and Spatiotemporal Binding Patterns. Below, all results are reported in the order NORMAL, $DISEASED_{CCl4}$ and, $DISEASED_{ALC}$, when values for all three are provided, and $DISEASED_{CCl4}$ and $DISEASED_{ALC}$ when only DISEASED ISL values are provided. There are no wet-lab methods to measure which lobular subspaces (within a particular lobule) are visited by a compound during a single pass through the liver. We recorded each COMPOUND'S SINUSOID traverse path (in grid spaces) for 100 SECONDS after dosing: until it either exited the LOBULE, was METABOLIZED, or the run ended. Path lengths were divided into two types: complete and incomplete. In the above order, the mean percent of the dose that ended at CV was 47, 59, and 38%, whereas 23, 9, and 29% ended at a SS (it was METABOLIZED). Passage was still in progress when the run ended for 30, 32, and 33% of the DILTIAZEM dose. SUCROSE had shorter path lengths because it did not enter CELLS and so was more likely to reach CV before the run terminated. The average path lengths for DILTIAZEM, in the above order, were 64, 59, and 55, whereas for sucrose the averages were 79, 65, and 76. The shorter mean path for DISEASED ISLs shows that both DISEASE types made it easier for COMPOUNDS to move closer to CV as TIME advanced. It is evident from Fig. 6a & b inserts that $DISEASED_{CCl4}$ ISLs had a more narrowly distributed variety of path lengths. Note also that the $DISEASED_{CCl4}$ ISLs had significantly fewer of the shortest paths (0–25 grid spaces) than either NORMAL or $DISEASED_{ALC}$ ISLs.

The data in Fig. 6c & d show that the fraction of COMPOUNDS that was in a LOBULE at a particular TIME and was attached to a BINDER eventually reached a similar steady state ratio of about 0.8 in $DISEASED_{CCl4}$ and $DISEASED_{ALC}$ LOBULES. However, the relative fractions BOUND in ENDOTHELIAL (Space B) and HEPATOCYTE layers (Space C) were different. In the order presented above, means (and SD) for the fraction bound within all CELLS were 0.60 (0.19), 0.67 (0.20), and 0.62 (0.17). The fraction bound within ENDOTHELIAL CELLS in Space B was 0.53 (0.18), 0.49 (0.16), and 0.59 (0.17); the fraction bound within HEPATOCYTES in Space C was 0.07 (0.02), 0.17 (0.04), and 0.03 (0.01).

Consistent with the parsimony guideline, everything within or around hepatocytes that was capable of binding or sequestering diltiazem was conflated and represented using one INTRACELLULAR BINDER type. Only a small subset of that material includes enzymes that metabolize diltiazem. Because of how events were scheduled, it is possible for a DILTIAZEM to be released toward the end of one simulation step and—by chance—be bound again to another BINDER in that same CELL before being given an opportunity to move out of the CELL.

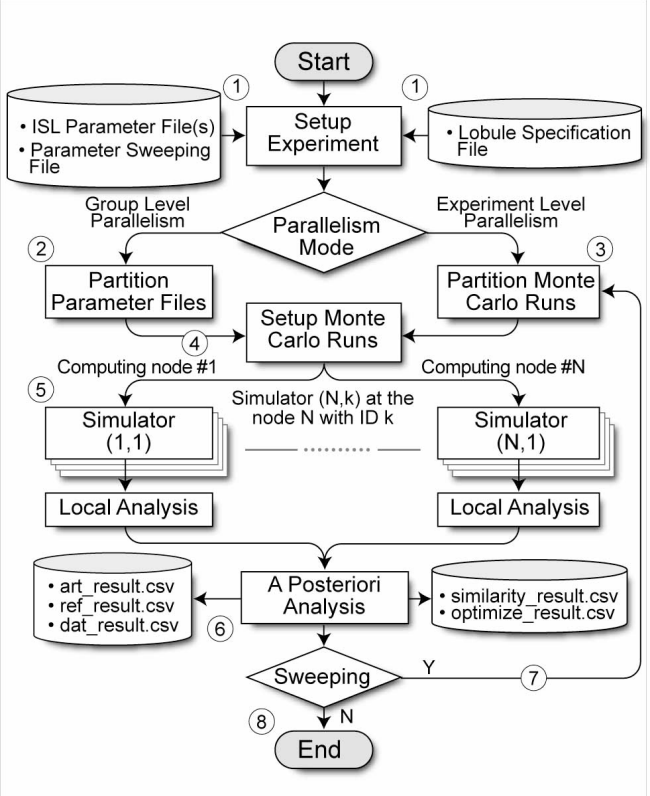

Figure S1. Lifecyle management of ISL experiments. There are eight stages. 1. An ISL experiment is configured with a LOBULE specification file that describes the structural topology of a LOBULE, an ISL parameter file that lists all parameters and their values, and a parameter-sweeping file that specifies a non-linear discrete region of ISL parameter space to be swept. A parameter sweeping space is a collection of ISL parameter files. They are dynamically constructed from ISL parameter and sweeping files by a parameter sweeper. The sweeping space is partitioned depending on the parallel mode selected. 2. The sweeping space is decomposed into a set of partition blocks in the Group Level Parallel mode, which is a coarse-grain parallelism. Parallel batch processing of multiple parameter files is performed in this mode. 3. A set of multiple Monte Carlo runs of a single parameter file is decomposed into a set of partition blocks in the Experiment Level Parallel mode, which is a fine-grain parallelism. 4. Partition blocks are dispatched to a set of computation nodes. 5. A simulator at each computation node runs concurrently using a parameter file or a collection of Monte Carlo runs depending on the parallel mode. 6. A posteriori analysis is conducted over the results produced concurrently by local analysis at each computation node. These two-phase analyses improve overall performance. All analytical results are stored within a shared file system. 7. If parameter sweeping is activated, ISL experiments are continued until all parameter sets in the sweeping space are consumed. 8. Otherwise, the experiment is stopped.

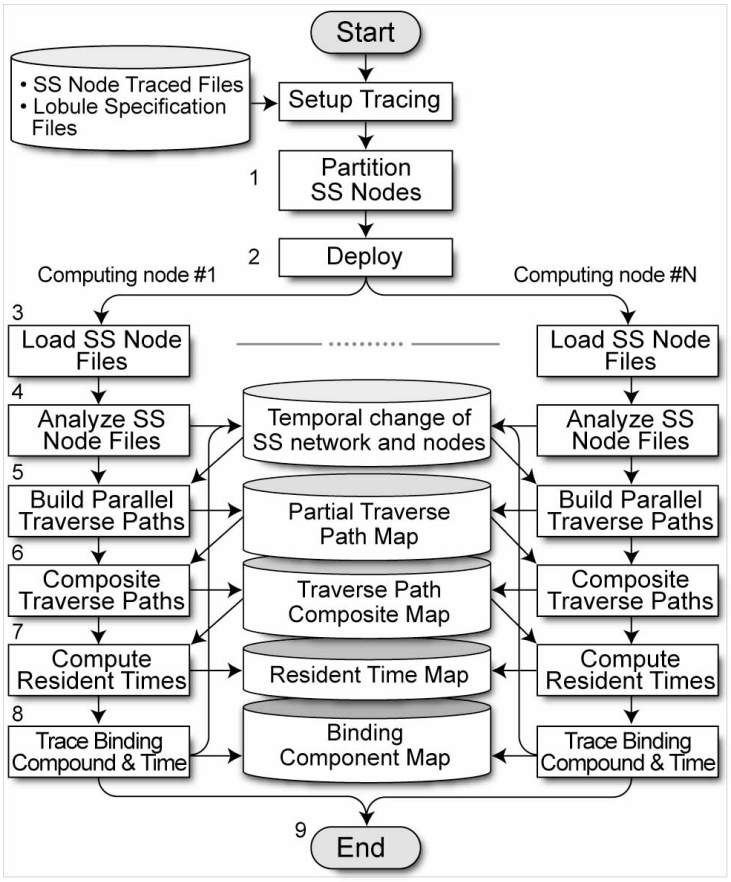

Figure S2. Multiscale COMPOUND tracing within an ISL during execution. There are nine stages. 1. All SS are decomposed into a set of partition blocks. 2. Each block is dispatched to a set of computation nodes. 3. Each computation node loads generated tracing data referenced by its SS identification. 4. The temporal changes within each SS are traced by analyzing the files. 5. The *partial* traverse path of each COMPOUND is built by reconstructing the changes in terms of SS visited by each COMPOUND. The path is constructed over only those SS in the block. 6. The *full* COMPOUND traverse path is computed by combining its partial (and local) traverse paths into a single global path. 7. Resident TIME is computed from the traverse path at all levels listed in Fig. 3. 8. ISL COMPONENTS that bind a COMPOUND are traced by analyzing the temporal changes within SS nodes. 9. The process stops once tracing resident TIMES is complete at every computation node.

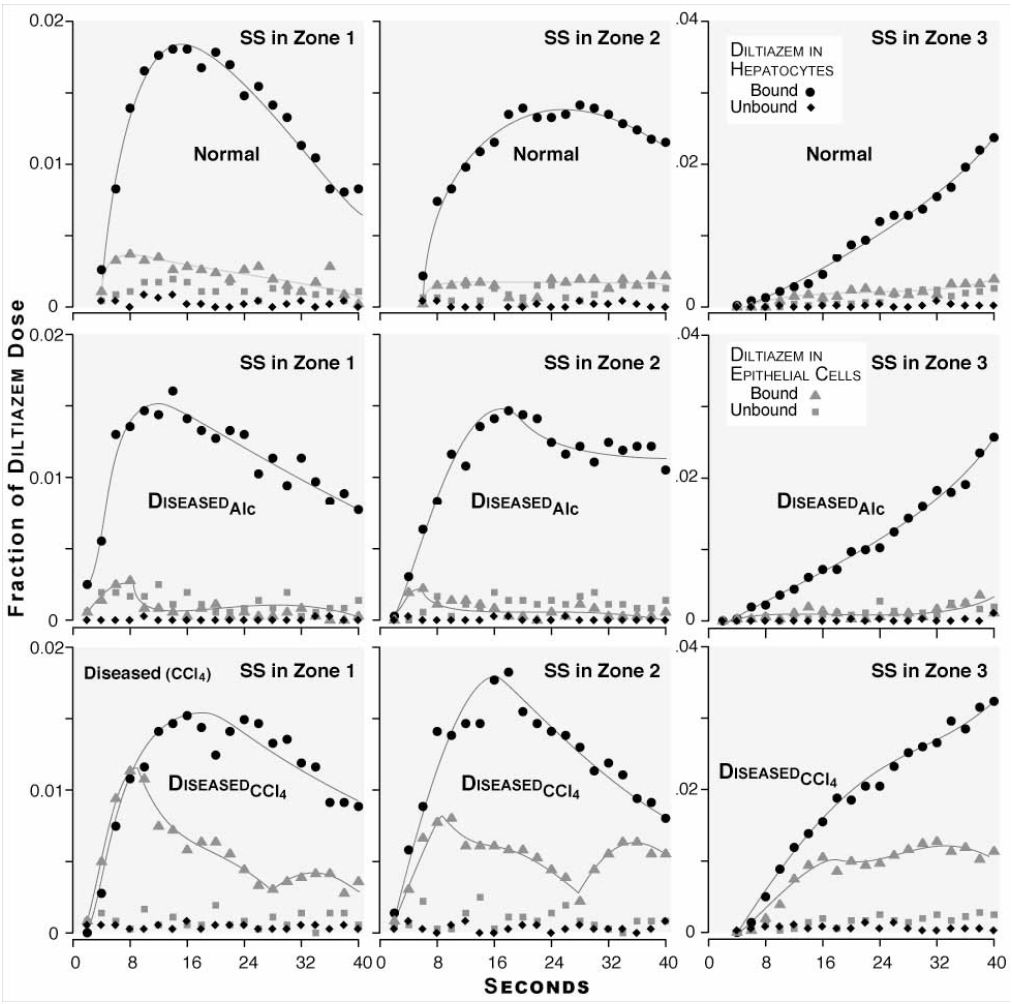

Figure S3. Fraction of DILTIZEM dose that was BOUND or UNBOUND within different SS spaces in each zone. The selected SSs were the same as those in manuscript Fig. 4. A comparable size SS was selected from Zone 1 (three left panels), Zone 2 (three center panels), and Zone 3 (three right panels) from a NORMAL (three top panels), a DISEASED$_{ALC}$ (three middle panels), and a DISEASED$_{CCl4}$ ISL (three bottom panels). In each panel, the dose fraction (regardless of location or state) that is BOUND or UNBOUND in HEPATOCYTES (in Space C) or in ENDOTHELIAL CELLS (in Spacxe B) at indicated times is plotted. The curves are approximate trend lines.

Supplementary Discussion

Relating Differences in ISL Parameter Values to Wet-Lab Measures of Disease. Microsomal protein and cytoskeleton residue are attributes of homogenized tissue samples and have no ISL counterparts. It is noteworthy, however, that *B2CJumpProb* in Fig. 4 exhibits the identical opposite trend for DISEASED$_{CCl4}$ and DISEASED$_{ALC}$ ISLs. Permeability (called the permeability-surface [PS] product by Hung et al. (2002a,b)) is a derived measure of water's ability to permeate lobular tissue. *A2BJumpProb* maps well to this measure. Number of fenestra counted fenestrae in comparable tissue sections. Fenestrae influence the ability of all material, especially larger material, to exit blood and access the space of Disse. The pattern of change in *A2BJumpProb* maps well to number of fenestra. In ISL Space B, an ENDOTHELIAL CELL is the lower limit or spatial resolution. Fenestrae are below that level of resolution and thus have no ISL counterpart. However, grid spaces not assigned to ENDOTHELIAL CELLS map to extracellular spaces, and so a

subset maps to FENESTRAE. If fenestrae are influential, then one might expect *ECDensity* to map inversely to number of fenestra (higher *ECDensity* → lower number of fenestra); but *ECDensity* is lower for $\text{DISEASED}_{\text{CCl4}}$ ISLs. However, there may well be different ISL parameterizations (mechanistic hypotheses) that also validate, in which the outward *JumpProb* parameter changes are lessened and *ECDensity* is changed to compensate. Additional ISL changes could be considered given semi-quantitative wet-lab data against which to validate. For example, a parameter can be added to reduce the fraction of COMPOUND-accessible extracellular spaces in Spaces B and C in DISEASED relative to NORMAL ISLs.

The albumin space measure decreased for both diseased livers. It is a measure of the lobular volume accessible to albumin. We might expect LOBULAR resident TIMES to map somewhat to accessible space: if the spaces are smaller, then resident time should decrease, and it did. We see in Fig. 5(a) that the SUCROSE and DILTIAZEM dose fractions having longer resident times decreased in both DISEASED ISLs. Membrane thicknesses are direct measures of representative hepatocyte membranes in tissues sections. There is no ISL counterpart because the CELL is the limit of resolution. It is not clear if membrane thickness plays any significant role in influencing cellular entry and exit of diltiazem. The reduction in *HepDensity* (and possibly *ECDensity*, also) maps directly to observed reductions in the number of functional hepatocytes in the CCl_4-treated livers.

Collagenization, which is increased in different ways in the two disease models, would be expected to make it harder for a compound to move "into" tissue spaces, and harder to return once there. In the DISEASED ISLs, movement between spaces, *A2BJumpProb*, etc. plus *SinusoidTurbo* (for $\text{DISEASED}_{\text{CCl4}}$ ISL), are altered. Their complex interactions influenced resident TIMES (Fig. 5) and path lengths (Fig. 6), which are reflected in the details of locations within and between Spaces observed in Fig. 4.

Supplementary References

de Hoog, F. R., Knight, J. H., and Stokes, A. N. (1982) An improved method for numerical inversion of Laplace transforms. *SIAM J Sci and Stat Comput* **3**: 357-366.

Hollenbeck, K. J. (1998) INVLAP.M: A MATLAB function for numerical inversion of Laplace transforms by the de Hoog algorithm. http://www.isva.dtu.dk/staff/karl/invlap.htm